4*c*). Taken together, these findings suggest that combined AdSOCS-1 and cisplatin plus pemetrexed activates caspase signaling pathways.

SOCS-1 gene delivery regulates NF-κB and STAT3 in MESO-4 and H226 cells

Because it has been reported that antiapoptotic signaling is regulated by the transcription factors NF-κB and STAT3, we investigated the role of AdSOCS-1 and cisplatin plus pemetrexed on NF-κB and STAT3 signaling in MESO-4 and H226 cells. NF-κB was stimulated by the inflammatory cytokine TNF-α (Fig. 5*a*). AdSOCS-1, but not cisplatin plus pemetrexed, inhibited phosphorylation and nuclear translocation of NF-κB stimulated by TNF-α in MESO-4 and H226 cells (Fig. 5*a*). In contrast, by NF-κB-dependent luciferase reporter assay and TransAM DNA-binding assay, we found that cisplatin plus pemetrexed cooperated with AdSOCS-1 to inhibit transcriptional and DNA-binding activity of NF-κB in MESO-4 and H226 cells (Fig. 5*d*). Regarding STAT3 regulation, AdSOCS-1, but not cisplatin plus pemetrexed, inhibited phosphorylation and transcriptional activity of STAT3 in MESO-4 and H226 cells (Figs. 5*b* and 5*d*). On the other hand, cisplatin plus pemetrexed cooperated with AdSOCS-1 to inhibit DNA-binding activity of STAT3 in MESO-4 and H226 cells (Fig. 5*d*). Furthermore, silencing NF-κB expression by siRNA abrogated XIAP in MESO-4 and H226 cells, whereas silencing STAT3 expression abrogated survivin in MESO-4 and H226 cells and FLIP in MESO-4 cells (Fig. 5*c*). Collectively, these data indicate that combined *SOCS-1* gene delivery and cisplatin plus pemetrexed exhibit antitumor effect in MESO-4 and H226 cells partially by inhibiting NF-κB and STAT3 signaling.

SOCS-1 gene delivery combined with cisplatin plus pemetrexed cooperates to exhibit antitumor activity in a mesothelioma xenograft model

We also evaluated the therapeutic effect of AdSOCS-1 combined with cisplatin plus pemetrexed on the growth of intrathoracically implanted MPM cells in ICR *nu/nu* mice. Of the MPM cell lines used in this study, we were able to establish MESO-4 and H226 xenograft models. Preliminary experiments revealed that when 1×10^6 MPM cells (MESO-4 or H226) were inoculated into the thoracic space, dissemination of tumors was observed in all mice 31 days after cell implantation. Injection of the AdSOCS-1 combined with cisplatin plus pemetrexed significantly reduced the weight of tumor nodules compared to the weight of those in control AdLacZ-injected animals (Fig. 6*b*). Furthermore, immunohistochemical analysis indicated that AdSOCS-1 inhibited nuclear translocation of NF-κB and AdSOCS-1 combined with cisplatin plus pemetrexed significantly induced apoptosis in the H226 tissue (Fig. 6*c*). However, apoptosis in MESO-4 tissue could not be clearly determined. From these results, we conclude that AdSOCS-1 combined with cisplatin plus pemetrexed exhibits antitumor activity not only *in vitro* but also *in vivo* in the MPM model. We hope that these findings may lead to the successful clinical application of SOCS-1 for MPM treatment.

Discussion

Malignant mesothelioma represents a great challenge to both clinicians and researchers because of its poor prognosis and remarkable resistance to current therapies. Although there have been some improvements in treatment over the past few years, a better understanding of the molecular basis of the disease and of how to improve treatment is required. In our study, we show that SOCS-1 is silenced in MPM cell lines, and *SOCS-1* gene delivery inhibits the proliferation of MPM cells through NF-κB and STAT3 pathways that promote antiapoptotic signaling. Specifically, we demonstrate that *SOCS-1* gene delivery cooperates with cisplatin plus pemetrexed to regulate NF-κB signaling and significantly to inhibit tumor growth of MPM *in vitro* and *in vivo*. These data provide new insights into the clinical application of *SOCS-1* gene delivery for the treatment of MPM.

In accordance with previous reports on several types of cells, we showed that AdSOCS1 regulated NF-κB signaling in MESO-4 and H226 cells. SOCS-1 was reported to ubiquitinate NF-κB p65.[15] We demonstrated that AdSOCS-1 suppressed the expression of nuclear NF-κB p65 in MESO-4 and H226 cells. Furthermore, we found that AdSOCS-1 inhibited phosphorylation of NF-κB p65 at Ser-536. Previous studies have demonstrated that phosphorylation of serine 536 in NF-κB p65 is necessary for transcriptional activity of NF-κB.[32,33] In addition to ubiquitination of NF-κB p65, SOCS-1 is known to interact with IL-1R–associated kinase (IRAK), a key molecule in the NF-κB pathway.[34] IRAK was reported to activate IκB kinase, which induced the phosphorylation of NF-κB p65 on Ser-536.[35] We also demonstrated that cisplatin plus pemetrexed inhibited the transcriptional activity of NF-κB p65 but did not affect its nuclear translocation. A previous study found that cisplatin did not affect NF-κB p65 nuclear translocation but modulated its transcriptional activity.[36] Taken together, our findings suggest that AdSOCS-1 cooperates with cisplatin plus pemetrexed to regulate NF-κB signaling by different mechanisms.

Consistent with previous studies on several types of cells, we found that AdSOCS-1 inhibited the phosphorylation of STAT3 at Tyr-705 in MESO-4 and H226 cells. On the other hand, we were not able to determine the effect of cisplatin plus pemetrexed on STAT3. Cisplatin plus pemetrexed did not affect the phosphorylation and transcriptional activity of STAT3, but inhibited DNA-binding activity of STAT3. A previous study indicated that cisplatin has minimal effects on STAT3 signaling.[37] Thus, we need further studies to clarify cisplatin plus pemetrexed involvement in the regulation of STAT3 signaling.

NF-κB and STAT3 are known to promote antiapoptotic signaling.[8] In MESO-4 and H226 cells, we found that NF-κB and STAT3 regulate antiapoptotic proteins survivin, XIAP in MESO-4 and H226 cells and FLIP in MESO-4 cells,

consistent with the results of previous studies.[38–40] The inhibition of these antiapoptotic proteins activates caspase-3, -8, and -9.[29] Taken together, our results suggest that *SOCS-1* gene delivery cooperates with cisplatin plus pemetrexed to induce apoptosis *via* NF-κB and STAT3 pathways.

We demonstrated that recombinant human active caspase-3 cleaved FAK and Akt and that combined *SOCS-1* gene delivery and cisplatin plus pemetrexed inhibited FAK and Akt expression in MPM cells. FAK and Akt are known to be the substrates of caspase-3.[41,42] Specifically, *SOCS-1* gene delivery and cisplatin plus pemetrexed strongly suppressed FAK expression in MPM cells. Interactions of SOCS-1 with FAK through the Src homology 2 domain have been reported to promote polyubiquitination and subsequent degradation of FAK.[43] We found that AdSOCS-1 significantly inhibited cell invasion in MPM cells. Because of an important role of FAK in cell invasion, we estimated that AdSOCS-1 strongly suppressed cell invasion partially through caspase and ubiquitin-mediated regulation of FAK.

In addition to NF-κB and STAT3 signaling, SOCS-1 is reported to regulate multiple signaling pathways including FAK, p38 MAPK and p53 pathways.[43–45] In our study, we consider that AdSOCS-1 inhibited cell growth in H28 cells partially by regulating these signaling pathways because NF-κB and STAT3 were not endogenously activated in H28 cells. On the other hand, the evidence for functional activity of SOCS-1 in tumor cell is controversial. SOCS-1 is reported to have different functions depending on types of tumor cells. For example, overexpression of SOCS-1 inhibits apoptosis in human acute T-cell leukemia cell lines (Jurkat cells).[46] Furthermore, SOCS-1 silencing suppresses cell proliferation and invasion in murine melanoma cells.[47] Therefore, the role of SOCS-1 in tumor progression is thought to be cell type specific.

In contrast, recently developed tyrosine kinase inhibitors (TKIs) tend to target specific abnormalities in cancer cells and exhibit surprising effects on patients having these abnormalities. For example, EGFR-TKIs, such as gefitinib, exhibit up to a 70% response rate against non-small cell lung cancer harboring somatic mutations of the EGFR gene.[48,49] These TKIs have been tested for MPM but without therapeutic benefit.[2] This is partially explained by the fact that multiple receptor tyrosine kinases are frequently activated in most MPM cells.[50] Therefore, SOCS-1, which regulates multiple signaling in different manners, is expected to be an attractive candidate for the treatment of MPM.

In this study, we examined only the cooperative effect of AdSOCS-1 and cisplatin plus pemetrexed. However, *SOCS-1* gene delivery combined with chemotherapeutics other than cisplatin plus pemetrexed might represent increased antitumor effect. It is of interest to investigate the effect of *SOCS-1* gene therapy combined with drugs such as gemcitabine, etoposide, doxorubicin and vinorelbine, because they have mechanisms of action distinct from those of cisplatin and pemetrexed. Moreover, these new combinations might be useful as second- or third-line therapies for patients with MPM with poor response to the first-line therapy, cisplatin plus pemetrexed. Further preclinical analyses are required to elucidate the optimal combination therapy with *SOCS-1* gene delivery and chemotherapeutics.

In conclusion, we demonstrated the antitumor effect of *SOCS-1* gene delivery in MPM. Furthermore, we showed the efficacy of combined *SOCS-1* gene delivery and cisplatin plus pemetrexed *in vitro* and *in vivo*. The results of the clinical application of SOCS-1 for MPM treatment are eagerly anticipated.

Acknowledgements

This work was supported by a Grant-in-Aid for Young Scientists (B) from the Ministry of Education, Culture, Sports, Science and Technology, Japan (K. Iwahori), a Grant-in-Aid from the Ministry of Health, Labour and Welfare, Japan (T. Naka) and a grant from the Kansai Biomedical Cluster Project in Saito, which is promoted by the Knowledge Cluster Initiative of the Ministry of Education, Culture, Sports, Science and Technology, Japan (T. Naka). The authors thank Y. Ito, N. Kawakami and Y. Kanazawa for their secretarial assistance.

References

1. Vogelzang NJ, Rusthoven JJ, Symanowski J, et al. Phase III study of pemetrexed in combination with cisplatin versus cisplatin alone in patients with malignant pleural mesothelioma. *J Clin Oncol* 2003;21:2636–44.
2. Kelly RJ, Sharon E, Hassan R. Chemotherapy and targeted therapies for unresectable malignant mesothelioma. *Lung Cancer* 2011;73:256–63.
3. Pelucchi C, Malvezzi M, La Vecchia C, et al. The mesothelioma epidemic in Western Europe: an update. *Br J Cancer* 2004;90:1022–4.
4. Leigh J, Driscoll T. Malignant mesothelioma in Australia, 1945–2002. *Int J Occup Environ Health* 2003;9:206–17.
5. Leithner K, Leithner A, Clar H, et al. Mesothelioma mortality in Europe: impact of asbestos consumption and simian virus 40. *Orphanet J Rare Dis* 2006;1:44.
6. Murayama T, Takahashi K, Natori Y, et al. Estimation of future mortality from pleural malignant mesothelioma in Japan based on an age-cohort model. *Am J Ind Med* 2006;49:1–7.
7. Grivennikov SI, Greten FR, Karin M. Immunity, inflammation, and cancer. *Cell* 2010;140:883–99.
8. Bollrath J, Greten FR. IKK/NF-κB and STAT3 pathways: central signalling hubs in inflammation-mediated tumour promotion and metastasis. *EMBO Rep* 2009;10:1314–19.
9. Janssen YM, Barchowsky A, Treadwell M, et al. Asbestos induces nuclear factor kappa B (NF-κB) DNA-binding activity and NF-kappa B-dependent gene expression in tracheal epithelial cells. *Proc Natl Acad Sci USA* 1995;92:8458–62.
10. Luster MI, Simeonova PP. Asbestos induces inflammatory cytokines in the lung through redox sensitive transcription factors. *Toxicol Lett* 1998;102/103:271–5.
11. Simeonova PP, Luster MI. Asbestos induction of nuclear transcription factors and interleukin 8 gene regulation. *Am J Respir Cell Mol Biol* 1996;15:787–95.
12. Endo TA, Masuhara M, Yokouchi M, et al. A new protein containing an SH2 domain that inhibits JAK kinases. *Nature* 1997;387:921–4.
13. Naka T, Narazaki M, Hirata M, et al. Structure and function of a new STAT-induced STAT inhibitor. *Nature* 1997;387:924–9.
14. Starr R, Willson TA, Viney EM, et al. A family of cytokine-inducible inhibitors of signalling. *Nature* 1997;387:917–21.
15. Ryo A, Suizu F, Yoshida Y, et al. Regulation of NF-κB signaling by Pin1-dependent prolyl isomerization and ubiquitin-mediated proteolysis of p65/RelA. *Mol Cell* 2003;12:1413–26.
16. Narazaki M, Fujimoto M, Matsumoto T, et al. Three distinct domains of SSI-1/SOCS-1/JAB protein are required for its suppression of interleukin 6 signaling. *Proc Natl Acad Sci USA* 1998;95:13130–4.

17. Yasukawa H, Misawa H, Sakamoto H, et al. The JAK-binding protein JAB inhibits Janus tyrosine kinase activity through binding in the activation loop. *EMBO J* 1999;18:1309–20.
18. Yoshikawa H, Matsubara K, Qian GS, et al. SOCS-1, a negative regulator of the JAK/STAT pathway, is silenced by methylation in human hepatocellular carcinoma and shows growth-suppression activity. *Nat Genet* 2001;28: 29–35.
19. Nagai H, Kim YS, Konishi N, et al. Combined hypermethylation and chromosome loss associated with inactivation of SSI-1/SOCS-1/JAB gene in human hepatocellular carcinomas. *Cancer Lett* 2002;186:59–65.
20. Fukushima N, Sato N, Sahin F, et al. Aberrant methylation of suppressor of cytokine signalling-1 (SOCS-1) gene in pancreatic ductal neoplasms. *Br J Cancer* 2003;89:338–43.
21. Galm O, Yoshikawa H, Esteller M, et al. SOCS-1, a negative regulator of cytokine signaling, is frequently silenced by methylation in multiple myeloma. *Blood* 2003;101:2784–8.
22. Oshimo Y, Kuraoka K, Nakayama H, et al. Epigenetic inactivation of SOCS-1 by CpG island hypermethylation in human gastric carcinoma. *Int J Cancer* 2004;112:1003–9.
23. Sterman DH, Recio A, Carroll RG, et al. A phase I clinical trial of single-dose intrapleural IFN-β gene transfer for malignant pleural mesothelioma and metastatic pleural effusions: high rate of antitumor immune responses. *Clin Cancer Res* 2007;13:4456–66.
24. Sterman DH, Recio A, Vachani A, et al. Long-term follow-up of patients with malignant pleural mesothelioma receiving high-dose adenovirus herpes simplex thymidine kinase/ganciclovir suicide gene therapy. *Clin Cancer Res* 2005;11: 7444–53.
25. Yamana J, Yamamura M, Okamoto A, et al. Resistance to IL-10 inhibition of interferon gamma production and expression of suppressor of cytokine signaling 1 in CD4+ T cells from patients with rheumatoid arthritis. *Arthritis Res Ther* 2004;6:R567–R577.
26. Mizuguchi H, Kay MA. A simple method for constructing E1- and E1/E4-deleted recombinant adenoviral vectors. *Hum Gene Ther* 1999;10: 2013–17.
27. Sakurai H, Tashiro K, Kawabata K, et al. Adenoviral expression of suppressor of cytokine signaling-1 reduces adenovirus vector-induced innate immune responses. *J Immunol* 2008;180: 4931–8.
28. Maizel JV, Jr, White DO, Scharff MD. The polypeptides of adenovirus. I. Evidence for multiple protein components in the virion and a comparison of types 2, 7A, and 12. *Virology* 1968;36:115–25.
29. Vucic D, Fairbrother WJ. The inhibitor of apoptosis proteins as therapeutic targets in cancer. *Clin Cancer Res* 2007;13:5995–6000.
30. Mita AC, Mita MM, Nawrocki ST, et al. Survivin: key regulator of mitosis and apoptosis and novel target for cancer therapeutics. *Clin Cancer Res* 2008;14:5000–5.
31. Bagnoli M, Canevari S, Mezzanzanica D. Cellular FLICE-inhibitory protein (c-FLIP) signalling: a key regulator of receptor-mediated apoptosis in physiologic context and in cancer. *Int J Biochem Cell Biol* 2010;42:210–13.
32. Zhong H, Voll RE, Ghosh S. Phosphorylation of NF-κB p65 by PKA stimulates transcriptional activity by promoting a novel bivalent interaction with the coactivator CBP/p300. *Mol Cell* 1998;1: 661–71.
33. Zhong H, May MJ, Jimi E, et al. The phosphorylation status of nuclear NF-κB determines its association with CBP/p300 or HDAC-1. *Mol Cell* 2002;9:625–36.
34. Nakagawa R, Naka T, Tsutsui H, et al. SOCS-1 participates in negative regulation of LPS responses. *Immunity* 2002;17:677–87.
35. Hayden MS, Ghosh S. Signaling to NF-κB. *Genes Dev* 2004;18:2195–224.
36. Campbell KJ, Witty JM, Rocha S, et al. Cisplatin mimics ARF tumor suppressor regulation of RelA (p65) nuclear factor-κB transactivation. *Cancer Res* 2006;66:929–35.
37. Turkson J, Zhang S, Palmer J, et al. Inhibition of constitutive signal transducer and activator of transcription 3 activation by novel platinum complexes with potent antitumor activity. *Mol Cancer Ther* 2004;3:1533–42.
38. Aoki Y, Feldman GM, Tosato G. Inhibition of STAT3 signaling induces apoptosis and decreases survivin expression in primary effusion lymphoma. *Blood* 2003;101:1535–42.
39. Haga S, Terui K, Zhang HQ, et al. Stat3 protects against Fas-induced liver injury by redox-dependent and -independent mechanisms. *J Clin Invest* 2003;112:989–98.
40. Stehlik C, de Martin R, Kumabashiri I, et al. Nuclear factor (NF)-κB-regulated X-chromosome-linked iap gene expression protects endothelial cells from tumor necrosis factor alpha-induced apoptosis. *J Exp Med* 1998;188: 211–16.
41. Wen LP, Fahrni JA, Troie S, et al. Cleavage of focal adhesion kinase by caspases during apoptosis. *J Biol Chem* 1997;272:26056–61.
42. Bachelder RE, Ribick MJ, Marchetti A, et al. p53 inhibits alpha 6 beta 4 integrin survival signaling by promoting the caspase 3-dependent cleavage of AKT/PKB. *J Cell Biol* 1999;147:1063–72.
43. Liu E, Cote JF, Vuori K. Negative regulation of FAK signaling by SOCS proteins. *EMBO J* 2003; 22:5036–46.
44. Calabrese V, Mallette FA, Deschenes-Simard X, et al. SOCS1 links cytokine signaling to p53 and senescence. *Mol Cell* 2009;36:754–67.
45. Souma Y, Nishida T, Serada S, et al. Anti-proliferative effect of SOCS-1 through the suppression of STAT3 and p38 MAPK activation in gastric cancer cells. *Int J Cancer*, in press.
46. Kimura A, Naka T, Nagata S, et al. SOCS-1 suppresses TNF-α-induced apoptosis through the regulation of Jak activation. *Int Immunol* 2004;16: 991–9.
47. Scutti JA, Matsuo AL, Pereira FV, et al. Role of SOCS-1 gene on melanoma cell growth and tumor development. *Transl Oncol* 2011;4:101–9.
48. Mok TS, Wu YL, Thongprasert S, et al. Gefitinib or carboplatin-paclitaxel in pulmonary adenocarcinoma. *N Engl J Med* 2009;361:947–57.
49. Rosell R, Moran T, Queralt C, et al. Screening for epidermal growth factor receptor mutations in lung cancer. *N Engl J Med* 2009;361:958–67.
50. Sekido Y. Genomic abnormalities and signal transduction dysregulation in malignant mesothelioma cells. *Cancer Sci* 2010;101:1–6.

Citation: Cell Death and Disease (2012) 3, e363; doi:10.1038/cddis.2012.106

www.nature.com/cddis

Adoptive transfer of Th1-conditioned lymphocytes promotes axonal remodeling and functional recovery after spinal cord injury

H Ishii[1,2,3], X Jin[1,2], M Ueno[1,2], S Tanabe[1,2], T Kubo[3], S Serada[4], T Naka[4] and T Yamashita*[,1,2]

The role of T lymphocytes in central nervous system (CNS) injuries is controversial, with inconsistent results reported concerning the effects of T-lymphocyte transfer on spinal cord injury (SCI). Here, we demonstrate that a specific T-lymphocyte subset enhances functional recovery after contusion SCI in mice. Intraperitoneal adoptive transfer of type 1 helper T (Th1)-conditioned cells 4 days after SCI promoted recovery of locomotor activity and tactile sensation and concomitantly induced regrowth of corticospinal tract and serotonergic fibers. However, neither type 2 helper T (Th2)- nor IL-17-producing helper T (Th17)-conditioned cells had such effects. Activation of microglia and macrophages were observed in the spinal cords of Th1-transfered mice after SCI. Specifically, M2 subtype of microglia/macrophages was upregulated after Th1 cell transfer. Neutralization of interleukin 10 secreted by Th1-conditioned cells significantly attenuated the beneficial effects by Th1-conditioned lymphocytes after SCI. We also found that Th1-conditioned lymphocytes secreted significantly higher levels of neurotrophic factor, neurotrophin 3 (NT-3), than Th2- or Th17-conditioned cells. Thus, adoptive transfer of pro-inflammatory Th1-conditioned cells has neuroprotective effects after SCI, with prospective implications in immunomodulatory treatment of CNS injury.

Cell Death and Disease (2012) **3,** e363; doi:10.1038/cddis.2012.106; published online 9 August 2012
Subject Category: Neuroscience

Immune reactions following central nervous system (CNS) trauma such as spinal cord injury (SCI) or traumatic brain injury have been considered harmful to axonal regeneration and functional recovery.[1–3] Immune cells secondarily attack even spared neurons that escape primary damage.[1,2,4] However, in the last decade, the improvement of motor function by adoptive transfer or activation of autoimmune T cells has also been reported after CNS injury.[5–10] Surprisingly, autoimmune cells originally considered pathogenic in autoimmune diseases (e.g. multiple sclerosis and rheumatoid arthritis) were indicated to be neuroprotective after CNS trauma. Furthermore, several studies have suggested that T cells were beneficial to disease progression and survival after the onset of amyotrophic lateral sclerosis.[11,12] In contrast, others have reported that T lymphocytes caused axonal damage after CNS injury[3,13,14] and that transfer of autoimmune T lymphocytes exacerbated functional recovery after SCI.[15] These seemingly contradictory findings may be explained by the distinct roles of each T-lymphocyte subset; some are beneficial and others are detrimental to functional recovery after CNS injuries. For example, interleukin-17 (IL-17)-producing $\gamma\delta$T cells were reported to have a pivotal role in the pathogenesis of ischemic brain injury.[16] Thus, elucidation of the distinct role of T-cell subsets may lead to new insights for therapeutic interventions that regulate immune reaction following CNS injury.

Subsets of helper T cells have been suggested to have a role in the etiology of CNS diseases. IFN-γ-producing type 1 helper T (Th1) cells and IL-17-producing helper T (Th17) cells are associated with the disease onset and progression of experimental autoimmune encephalomyelitis (EAE), an animal model of multiple sclerosis.[17] Shift to IL-4-producing type 2 helper T (Th2) cells was suggested to lead to enhanced functional recovery after CNS injury.[18] However, knowledge of the role played by each T-lymphocyte subset is still fragmental, and the effectiveness of transferring specific T lymphocytes to treat CNS injury remains unknown. In the present study, we hypothesized that conflicting results concerning the role of T lymphocytes in recovery from CNS injury may be attributed to differences in the role of helper T-cell subsets, specifically that the transfer of pro-inflammatory Th1 cells could facilitate functional recovery

[1]Department of Molecular Neuroscience, Graduate School of Medicine, Osaka University, Suita, Osaka 565-0871, Japan; [2]JST, CREST, Chiyoda-ku, Tokyo 102-0075, Japan; [3]Department of Neurobiology, Graduate School of Medicine, Chiba University, Chuo-ku, Chiba 260-8677, Japan and [4]Laboratory for Immune Signal, National Institute of Biomedical Innovation, Ibaraki, Osaka 565-0085, Japan
*Corresponding author: T Yamashita, Department of Molecular Neuroscience, Graduate School of Medicine, Osaka University, 2-2 Yamadaoka, Suita, Osaka 565-0871, Japan. Tel: +81 6 6879 3661; Fax: +81 6 6879 3669; E-mail: yamashita@molneu.med.osaka-u.ac.jp
Keywords: Th1 cells; spinal cord injury; axonal sprouting
Abbreviations: CNS, central nervous system; SCI, spinal cord injury; IL-10, interleukin 10; Th1 cells, type 1 helper T cells; Th2 cells, type 2 helper T cells; Th17, IL-17-producing helper T cells; CD4, cluster of differentiation 4; PBS, phosphate-buffered saline; CST, corticospinal tract; BDA, biotin-dextran amine; 5-HT, 5-hydroxytryptamine; GFAP, glial fibrillary acidic protein; Arg1, Arginase 1; BDNF, brain-derived neurotrophic factor; NT-3, neurotrophin-3; GDNF, glia-derived neurotrophic factor; ELISA, enzyme-linked immunosorbent assay
Received 09.12.11; revised 13.6.12; accepted 03.7.12; Edited by A Verkhratsky

after CNS injury, as we previously identified that cocultured Th1-conditioned lymphocytes promote neurite outgrowth from cortical neurons.[19] Here, we report that the transfer of Th1-conditioned cells, but not Th2- or Th17-conditioned cells, facilitated recovery of sensorimotor function after SCI.

Results

Adoptive transfer of Th1-conditioned cells improves motor performance and tactile sensation after SCI. We assessed whether transfer of Th1-, Th2-, or Th17-conditioned lymphocytes *ex vivo* modulated disease progression in a mouse model of SCI. We isolated cluster of differentiation 4^+ ($CD4^+$) T cells from mice spleens and then cultured them to induce differentiation into each subset of helper T cells *in vitro*. Intracellular cytokine staining revealed differentiation into Th1, Th2 (Figure 1a), and Th17 cells (Figure 1b). As T cells in C57BL/6J mice congenitally tend to skew into Th1 cells,[20] we observed comparatively enriched Th1 cells in Th1-conditioned cells (Figure 1a, left). The efficiencies we observed were similar to that reported previously.[20–22]

Mouse spinal cords were contused at the level between thoracic vertebrae 9 (Th.9) and Th.10 by an impactor with a force of 60 kilodyne. All of the spinally injured mice became completely paraplegic on the first day after the injury, gradually displaying partial recovery of locomotor behavior. We carried out adoptive transfer of 5.0×10^6 Th1- or Th2-conditioned cells, which were activated with anti-CD3 and anti-CD28 antibodies for 3 h before the injection, at 4 days after SCI, and observed recovery of motor function as assessed by Basso Mouse Scale (BMS). The motor recovery

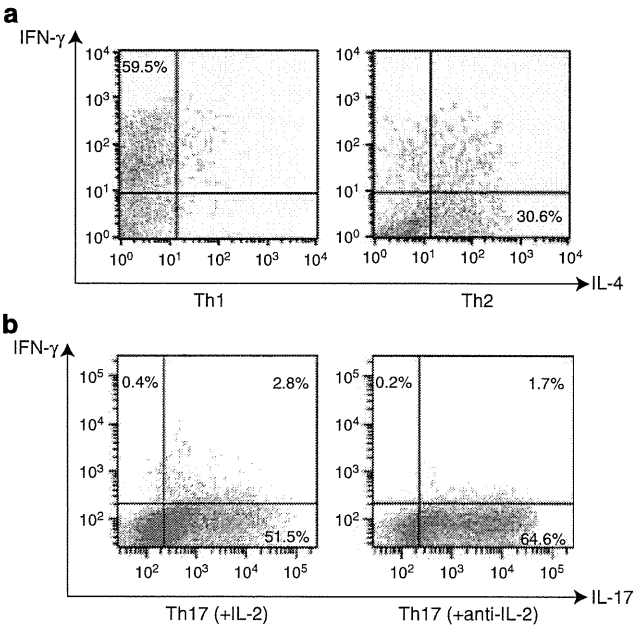

Figure 1 Intracellular staining of cytokines in cultured helper T-cell subsets. (**a**) Cytokine profile of Th1- and Th2-conditioned cells differentiated *in vitro*. (**b**) Cytokine profile of Th17-conditioned cells differentiated *in vitro* in the presence of IL-2 (left) or anti-IL-2 neutralizing antibody (right). Representative data are shown from two to three independent experiments

was transiently but significantly higher from 2 to 5 weeks after SCI in mice in which Th1-conditioned cells, but not Th2-conditioned cells, were transferred compared with phosphate-buffered saline (PBS)-injected mice (Figure 2a). We then increased the number of transferred T cells to maintain the effect of the transferred cells in the chronic phase. After the adoptive transfer of 1.0×10^7 Th1-conditioned cells, the mice showed significantly better motor performance after SCI than did PBS-injected SCI mice during the observation period up to 10 weeks (Figure 2b). Again, no difference was observed between mice transferred with Th2 cells and control mice (Figure 2b). Because cultured helper T cells are often restimulated for longer than 24 h,[23] we addressed whether longer restimulation leads to enhanced recovery. Adoptive transfer of Th1-conditioned cells that had been restimulated with anti-CD3/anti-CD28 antibodies for 24 h, longer than 3 h, into mice on day 5 after SCI also promoted the recovery (Figure 2c). However, the recovery level was similar to that shown in Figure 2b. The result suggests that cultured Th1-conditioned cells that were restimulated for 3 h were adequately activated.

We hypothesized that Th17 cells, which have been implicated in the pathology of EAE,[17] might exacerbate functional recovery after SCI. More than 50% of Th17-conditioned cells that were cultured in the presence of IL-2 differentiated into Th17 cells (Figure 1b, left). The hindlimb locomotor performance of mice intraperitoneally (i.p.) injected with Th17-conditioned cells did not show improvement compared with that of control mice (Figure 2b). As IL-2 may have negative effects on Th17 differentiation,[24] we added anti-IL-2 neutralizing antibody to the culture to promote Th17 differentiation (Figure 1b, right). When these Th17-conditioned cells were transferred after SCI, motor recovery was transiently exacerbated on day 7 after SCI (Figure 2d).

Consistent results were obtained when we performed the inclined plane task, which is considered to correlate with rubrospinal tract integrity, after SCI (Figure 2e). Thus, transfer of Th1-conditioned cells effectively enhanced motor recovery after SCI.

We next assessed tactile sensation by applying von Frey monofilaments to the plantar surface of the hindpaws. We tested hindpaw withdrawal thresholds in response to a sequence of ascending mechanical stimuli of increasing force. We observed significantly better improvement of tactile sensation at day 70 after SCI in mice with transfer of Th1 cells compared with control mice (Figure 2f). Thus, adoptive transfer of Th1-conditioned cells enhanced amelioration of sensory function after SCI.

Adoptive transfer of Th1-conditioned cells promotes remodeling of the injured corticospinal tract and raphespinal tract, and facilitates myelination after SCI. We assumed that the treatment promoted restoration of the neural network for motor function. We examined axonal regrowth of the descending corticospinal tract (CST) by injecting biotin-dextran amine (BDA) into sensorimotor cortices. We observed axon arbors extending from the main CST into the gray matter rostral to the lesion site in both mice with Th1-conditioned cell transfer and control mice in the

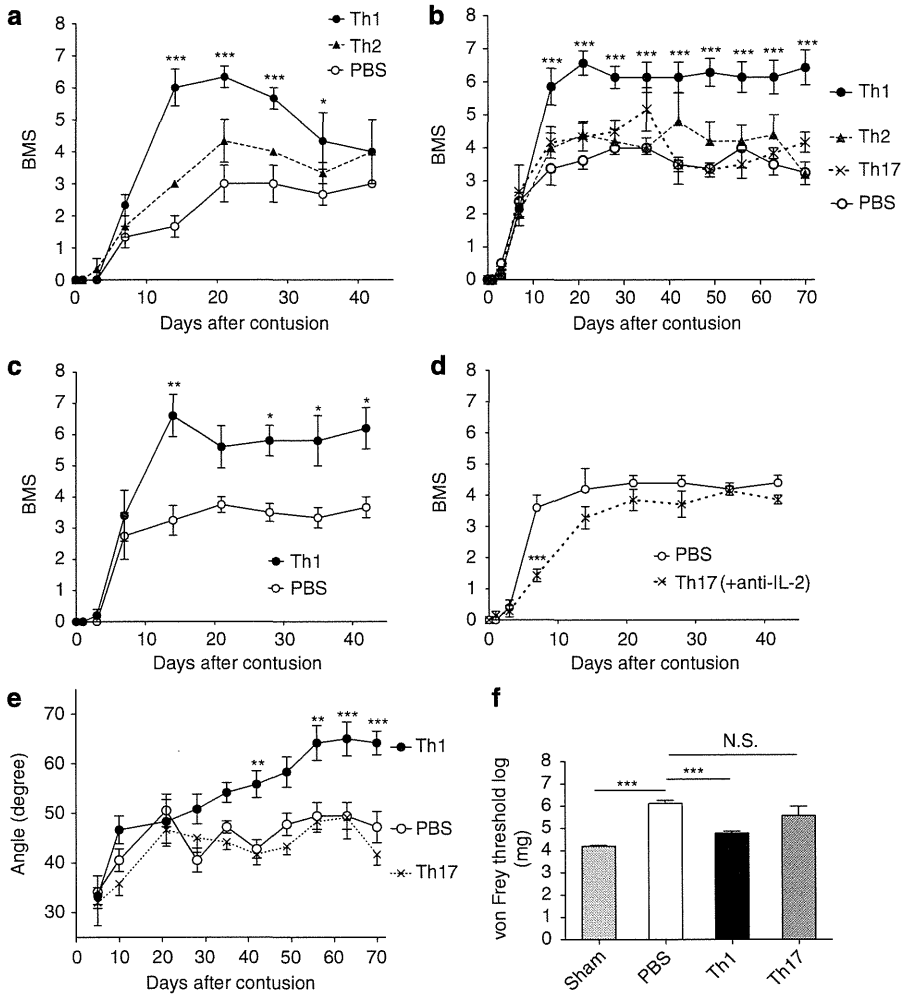

Figure 2 Transfer of Th1-conditioned cells ameliorates functional recovery after spinal cord injury (SCI). (**a**) BMS scores are shown for SCI mice after the transfer of 5.0×10^6 Th1- or Th2-conditioned cells (PBS, $n=3$; Th1, $n=3$; Th2, $n=3$). (**b**) Time course of hindlimb locomotion scored by BMS with adoptive transfer of 1.0×10^7 each helper T-cell subsets. Transfer of Th1-conditioned cells improved BMS score after SCI (PBS, $n=8$; Th1, $n=7$; Th2, $n=5$; Th17, $n=6$). (**c**) Time course of BMS scores after SCI followed by transfer of Th1-conditioned cells stimulated with anti-CD3/anti-CD28 antibodies for 24 h (PBS, $n=4$; Th1, $n=5$). (**d**) Time course of BMS scores for SCI mice after the transfer of anti-IL-2 antibody-treated Th17-conditioned cells (PBS, $n=5$, Th17 + anti-IL-2, $n=7$). (**e**) Time course of the inclined plane task. Th1-conditioned cells improved the angle of the inclined plane task (PBS, $n=9$; Th1, $n=6$; Th17, $n=6$). (**f**) Tactile sensation scored using the von Frey threshold at day 70 after SCI. Th1-conditioned cells improved tactile sensation after SCI. Sham SCI, $n=4$; PBS, $n=5$; Th1, $n=4$; Th17, $n=3$. Data are mean ± S.E.M. $^*P<0.05$, $^{**}P<0.01$, $^{***}P<0.001$; N.S., not significant *versus* the PBS group (two-way ANOVA with repeated measures, Bonferroni post-test (analysis of motor function-score) or one-way ANOVA with Dunnett post-test (analysis of sensory function-score))

transverse plane (Figure 3a). CST sprouting was quantitatively evaluated by the percentage of BDA-positive area compared with 5 mm rostral from the injured site. We did not detect BDA-positive fibers at or more than 1 mm caudal to the injured site in either group of mice (Figure 3b); this finding revealed that the lesion completely transected the axons in the descending CST. On the basis of quantitative analysis of the reconstructed spinal cord, we concluded that transfer of Th1 cells significantly enhanced axon sprouting of the CST rostral to the injured site after SCI.

As the serotonergic raphespinal tract contributes to motor function,[25] we assessed regrowth of descending serotonergic raphespinal tract axons using anti-5-hydroxytryptamine (anti-5-HT) immunostaining at 6 weeks after SCI (Figures 3c–f). Regrowth of raphespinal tract fibers was evaluated by 5-HT-positive area compared with 5 mm rostral from the injured site and measuring the 5-HT-positive fibers at 1 mm intervals rostral or caudal to the lesion epicenter. More 5-HT-positive fibers were observed in the spinal cord caudal to the injured site in Th1-treated mice than in PBS-injected mice, demonstrating that transfer of Th1-conditioned cells enhanced the growth of serotonergic nerve fibers after SCI (Figures 3c and d). We observed no difference in the 5-HT-positive area at 5 mm rostral to the injured site between the 2 groups (Figures 3e and f). These results support our notion that transfer of Th1-conditioned cells promotes remodeling of injured axons, thus leading to enhanced locomotor recovery after SCI.

To evaluate lesion size and tissue sparing, we carried out immunohistochemistry for glial fibrillary acidic protein (GFAP) at 6 weeks after SCI, and assessed the lesion area that was delineated by reactive astrocytes that were

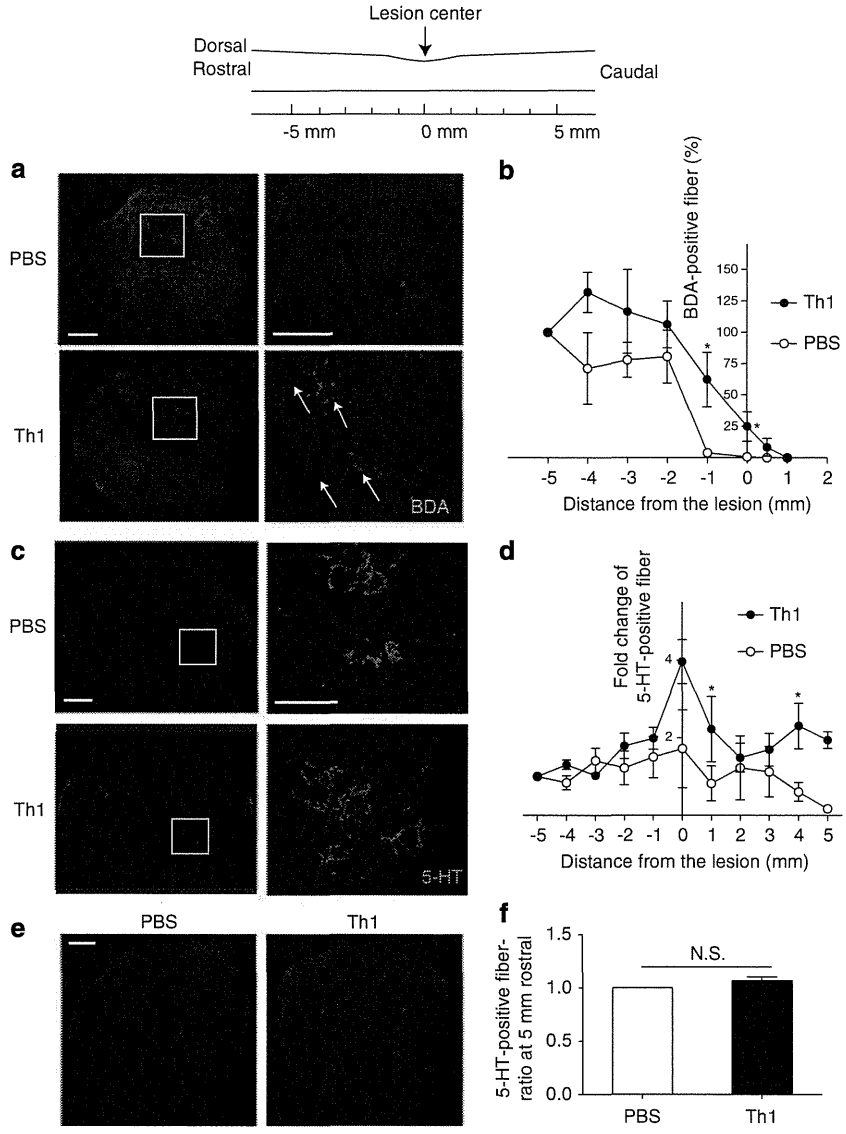

Figure 3 Transfer of Th1-conditioned cells promotes sprouting of the CST and raphespinal tract, and myelination after sSCI. The injured spinal cord is schematically illustrated (upper panel). (**a**) Representative images of BDA-labeled CST fibers (green) in transverse sections of the lesion epicenter; the pictures on the right are higher magnification views of the boxed regions of the pictures on the left. Arrows indicate sprouting fibers of a contused spinal cord into which the Th1-conditioned cells were transferred. Scale bar: left, 200 μm; right, 100 μm. (**b**) Quantification of the extent of CST growth/sprouting. The *x*-axis represents specific locations along the rostrocaudal axis of the spinal cord; the *y*-axis indicates the ratio of the average pixel number of axons at each rostrocaudal location outside the main CST to the pixel number of labeled fibers in the region 5 mm rostral to the lesion epicenter. Transfer of Th1-conditioned cells increased the sprouting of CST after SCI. PBS, control ($n=4$); Th1, transfer of Th1 ($n=6$). (**c**) Representative images of 5-HT-labeled fibers (red) in transverse sections 1 mm caudal to the lesion site; pictures on the right are higher magnification views of the boxed regions of the pictures on the left. Scale bar: left, 200 μm; right, 100 μm. (**d**) Quantification of 5-HT-positive fibers compared with those 5 mm rostral from the lesion site. Transfer of Th1-conditioned cells promoted raphespinal tract growth after SCI. PBS, control ($n=5$); Th1, transfer of Th1 ($n=7$). Scale bar: 200 μm. (**e**) Representative images of 5-HT-labeled fibers 5 mm rostral to the lesion site. (**f**) Quantification of the ratio of the 5-HT-positive area 5 mm rostral to the lesion site in Th1-transferred mice to that in PBS-treated mice ($n=4$ pairs of PBS/Th1). N.S., not significant (Paired *t* test). $^*P<0.05$ *versus* the control group (Mann–Whitney *U* test)

positive for GFAP. We observed no difference in the lesion shape, the lesion size, or the size of the spared tissues between PBS-injected mice and Th1 cell-transferred mice (Figures 4a–c).

Spared myelination is a hallmark of protective effects on injured neural networks. We performed myelin staining of spinal cord transverse sections at 6 weeks after SCI using FluoroMyelin (Figures 4d and e). We assessed the percentage of FluoroMyelin-positive myelinated area relative to the total area of white matter measured at 3 mm rostral to the lesion site. In both PBS-injected and Th1-transfer groups, the highest degree of demyelination occurred at the epicenter (Figure 4e). However, quantification of the data demonstrated that myelinated area was increased around the epicenter in mice undergoing Th1-conditioned cell transfer compared with control mice (Figures 4d and e). These results suggest that the Th1-conditioned cell transfer attenuated secondary damage and protected myelin after SCI.

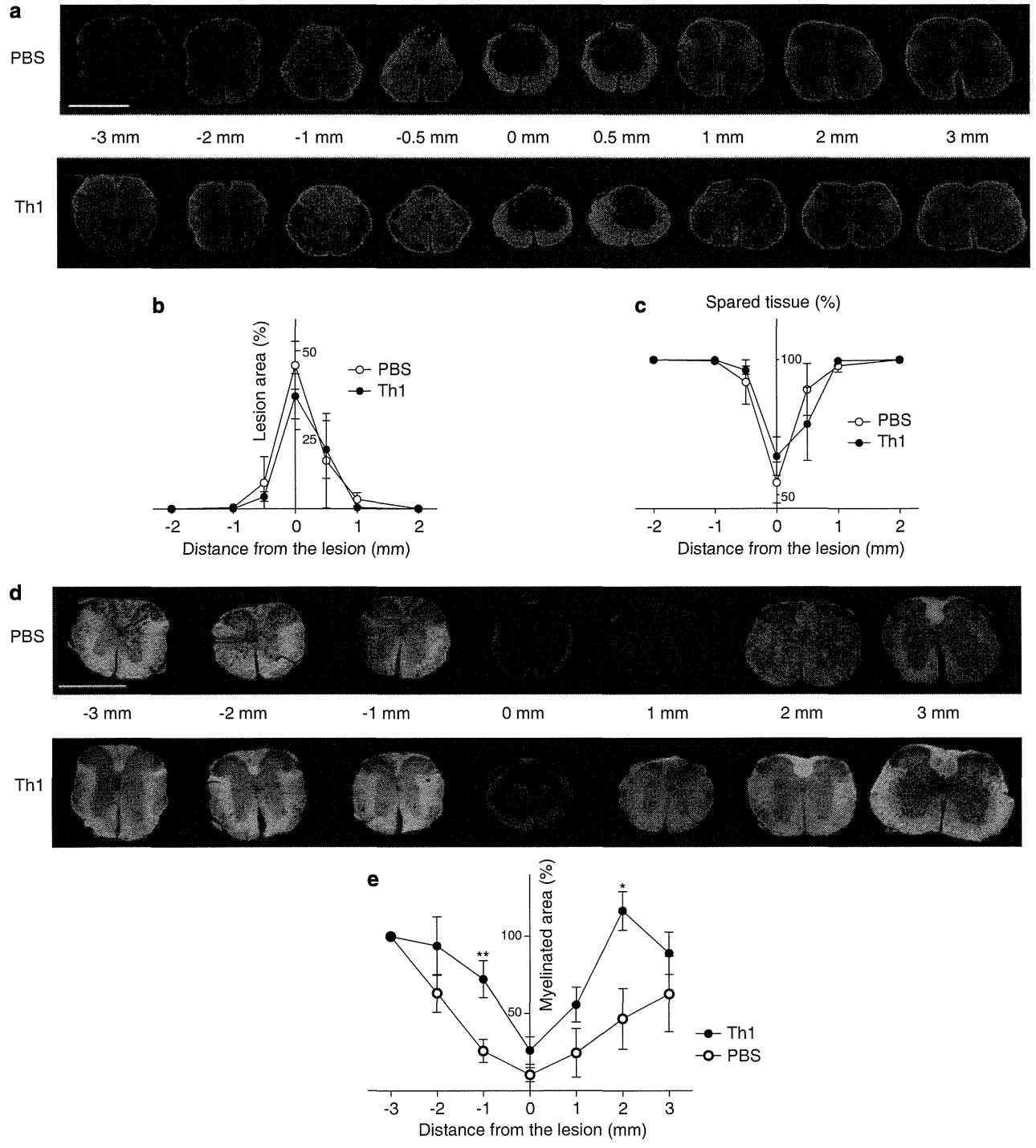

Figure 4 (**a**) Representative cross-sections of the spinal cords at the indicated distance from the lesion epicenter. These sections were immunostained for GFAP. Scale bar: 500 μm. (**b**) Quantification of the lesion area surrounded by reactive astrocytes in the cross-sections at the indicated distance from the lesion epicenter. PBS, control ($n=4$); Th1, transfer of Th1 ($n=4$). (**c**) Quantification of the spared tissue in the spinal cord. PBS, control ($n=4$); Th1, transfer of Th1 ($n=4$). No significant differences were observed (**b** and **c**, Mann–Whitney *U* test). (**d**) Staining of spared myelin sheath using FluoroMyelin. Scale bar: 500 μm. (**e**) Quantification of the FluoroMyelin-positive area compared with that 3 mm rostral from the lesion epicenter. Transfer of Th1-conditioned cells improved myelination after SCI. PBS, control ($n=6$); Th1, transfer of Th1 ($n=7$). $^{*}P<0.05$, $^{**}P<0.01$ *versus* the control group (Mann–Whitney *U* test)

Adoptive transfer of Th1-conditioned cells upregulates M2 subtype of microglia and macrophages after SCI. To elucidate the mechanistic basis of the effects induced by Th1-conditioned cell transfer, we analyzed immune cell accumulation in the injured spinal cord. We observed that more than 3.0×10^6 leukocytes infiltrated the injured spinal cord at day 4 after SCI (Figure 5a). Because beneficial role of microglia and macrophages in the CNS have been

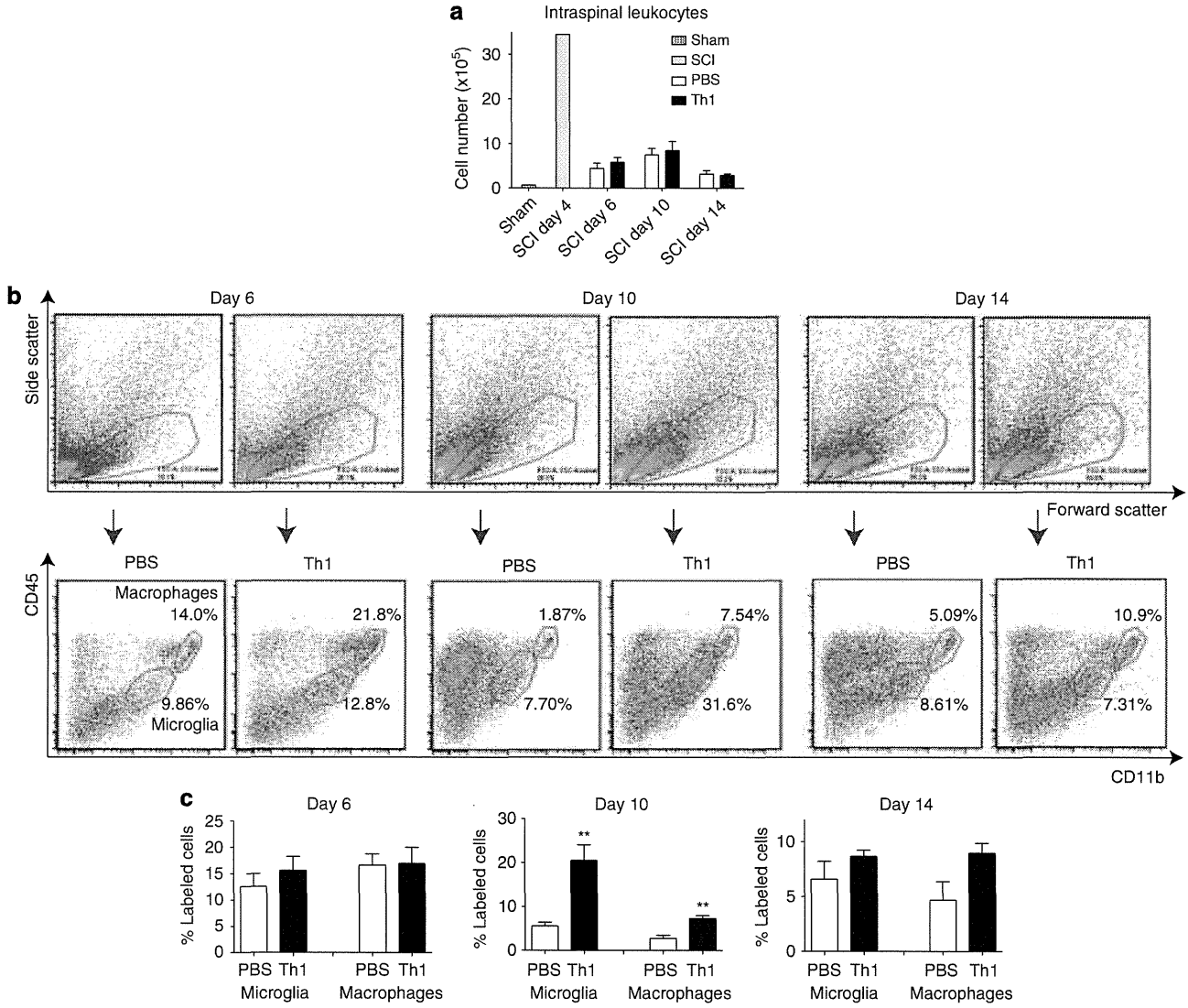

Figure 5 Increase of microglia/macrophages induced by adoptive transfer of Th1-conditioned cells after SCI. (**a**) Time course of leukocyte infiltration into the injured spinal cord. Th1-conditioned cells or PBS were injected i.p. on day 4 after SCI. (**b**) Representative profile of flow cytometric analysis of microglia/macrophages accumulated in the spinal cord on SCI days 6, 10, and 14 (2, 6, and 10 days, respectively, after PBS injection or Th1 cell transfer) of PBS or Th1-conditioned cells. Upper dot plots indicate side-scatter/forward-scatter profile by which CD11b/CD45 profiles were gated. In lower dot plots, $CD11b^{intermediate}$ $CD45^{intermediate}$ corresponds to microglia, whereas $CD11b^{high}$ $CD45^{high}$ corresponds to macrophages. (**c**) Quantification of microglia/macrophages accumulated in the injured spinal cord. Leukocytes isolated from the spinal cords of 2–4 mice were analyzed in each experiment. Representative data are shown from 3–4 independent experiments. $^{**}P<0.01$ *versus* the control group (Student's *t* test)

reported,[26–28] we investigated the profile of microglia and macrophages after SCI by evaluation of CD11b and CD45 immunoreactivity, with a fluorescence-activated cell sorter. The dot plots revealed that microglia and macrophages increased with Th1-conditioned cell transfer on day 10 after SCI (Figures 5b and c). Microglia/macrophages can be classified into two subtypes: pro-inflammatory M1 and anti-inflammatory M2.[28,29] The M1 subtype is considered to express neurotoxic effects, whereas the M2 subtype is considered to exhibit neuroprotective effects after a central nervous system injury. We performed flow cytometry by employing antibodies against markers for M1 (CD86 and IL-6) and M2 (CD206 and Arginase 1 (Arg1)) subtypes. Although the number of M1 marker-positive cells was not changed after Th1 transfer (data not shown), the number of $CD206^+$ cells among the macrophages increased at 10 days after SCI (Figures 6a and b). In addition to $CD206^+$ cells, the number of $Arg1^+$ cells among the microglia increased after Th1 transfer at 10 and 14 days after SCI (Figures 6c and d). These flow cytometry analyses demonstrated that Th1 cell transfer after SCI upregulated M2 subtype of microglia/macrophages.

IL-10 produced by Th1-conditioned cells is necessary for the recovery after SCI. As Th1 cells are reported to express IL-10,[30] which is known to be cerebroprotective[29] and IL-10 expression in Th1-conditioned cells was observed (Figure 7a, right), we addressed whether IL-10 was required for the effects of Th1-conditioned cells on recovery from SCI. Th1-conditioned cells were restimulated with

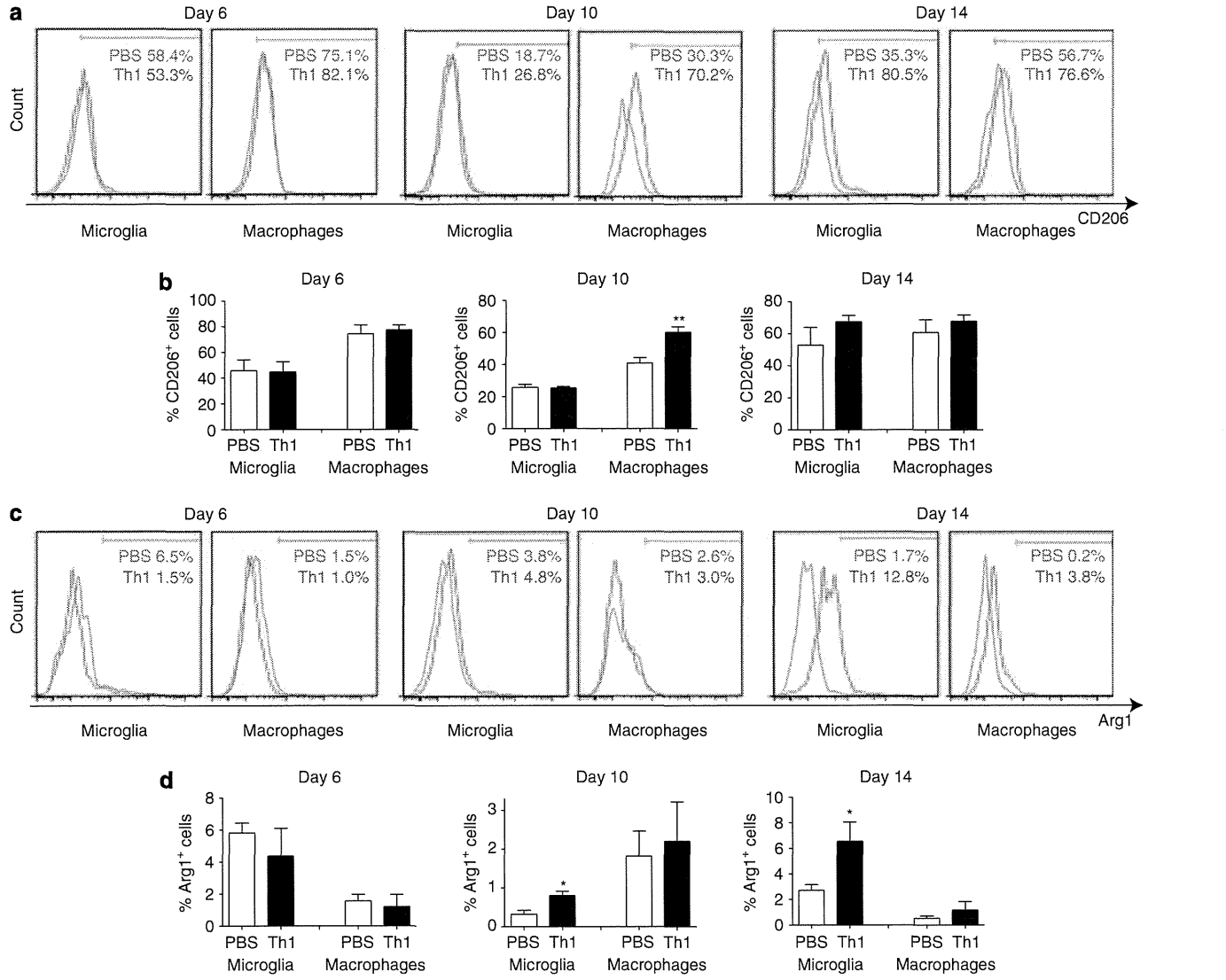

Figure 6 Transfer of Th1-conditioned cells after SCI promotes upregulation of M2 microglia/macrophages. (**a**) Histograms of CD206 expression on microglia and macrophages after SCI. (**b**) Quantification of CD206$^+$ microglia/macrophages at the indicated days after SCI. (**c**) Histograms of Arg1 expression on microglia and macrophages after SCI. (**d**) Quantification of Arg1$^+$ microglia/macrophages at the indicated days after SCI. $n=3$–4. All the data of the histograms were gated from the populations of microglia or macrophages as shown in Figure 5b. $^*P<0.05$, $^{**}P<0.01$ *versus* control group (Student's *t* test)

anti-CD3/anti-CD28 antibodies, simultaneously treated with anti-IL-10 neutralizing antibody, and then adoptively transferred with the antibody at day 4 after SCI, followed by injection of anti-IL-10 antibody i.p. at days 5, 7 and 11. Anti-IL-10 antibody treatment significantly attenuated the effect of Th1-conditioned lymphocytes (Figure 7b). This result demonstrates that IL-10 in Th1-conditioned lymphocytes is necessary for the promotion of functional recovery from SCI.

Th1-conditioned lymphocytes secrete neurotrophic factors. To find candidate molecules in Th1-conditoned cells responsible for axonal sprouting after contusion SCI, we assessed the expression of neurotrophic factors such as brain-derived neurotrophic factor (BDNF), neurotrophin-3 (NT-3), and glia-derived neurotrophic factor (GDNF) with enzyme-linked immunosorbent assay (ELISA) because they were reported to be expressed in activated T cell.[6] The expression level of NT-3 was higher in Th1 cells than in Th2 or Th17 cells (Figure 8a). However, BDNF expression was under the detection level among any T cell subsets (data not shown). Expression levels of GDNF in Th1- and Th2-conditioned cells were higher than that of Th17-conditioned cells (Figure 8b), but the absolute amount was around 30 pg/ml, which was much smaller than that of NT-3.

Discussion

The efficacy of T-lymphocyte transfer after CNS injury has been controversial,[18,31] and the detailed phenomena and mechanisms underlying the intervention are poorly understood. In the present study, we addressed our hypothesis that the beneficial and harmful effects of transferred T cells could

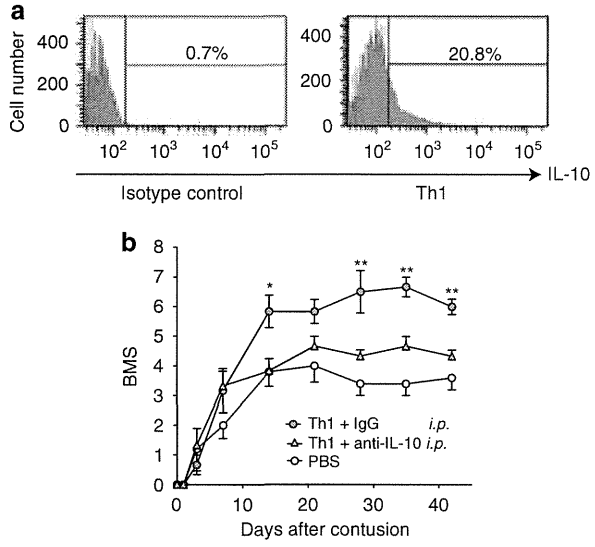

Figure 7 Expression of IL-10 in Th1-conditioned cells contributes to functional recovery after SCI with adoptive transfer of Th1-conditoned cells. (**a**) IL-10 expression in Th1 cells is shown as representative histograms from two independent experiments. (**b**) BMS scores in SCI mice with transfer of Th1-conditioned cells. These Th1-conditioned cells and mice were treated with control IgG or anti-IL-10 antibody (PBS, $n=5$; Th1 + IgG, $n=6$; and Th1 + anti-IL-10, $n=6$). $^*P<0.05$; $^{**}P<0.01$ *versus* anti-IL-10 + Th1 group (two-way ANOVA with repeated measures, Bonferroni post-test)

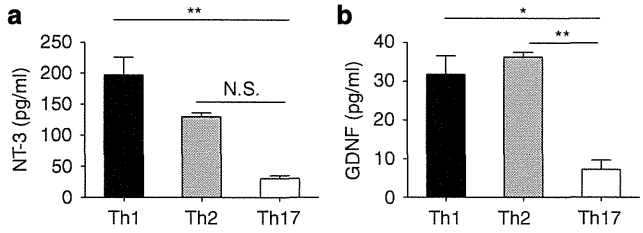

Figure 8 Expression of neurotrophic factors in subsets of T cells. NT-3 (**a**) and GDNF (**b**) in the supernatant of Th1, Th2, and Th17 cells detected by ELISA (Th1, $n=6$; Th2, $n=3$; Th17, $n=3$). $^*P<0.05$; $^{**}P<0.01$; N.S., not significant (one-way ANOVA with Dunnett post-test)

be explained by the distinct roles of helper T-cell subsets. Adoptive transfer of cultured Th1-conditioned cells into mice improved functional recovery after SCI. Although Th2 cells were suggested to be beneficial after CNS injury,[18] this was not the case in our experimental paradigm. Recovery of hindlimb locomotion by Th1 transfer after SCI coincides with improved neuronal network associated with motor function. Activation of monocytes by Th1 cell transfer may have a role in improved CST sprouting and myelination after SCI, as monocyte-derived cells are required for remyelination after toxin-induced demyelination[32] or EAE.[26]

The reported detrimental effects of T cells after CNS trauma[14,15] may be due to the function of specific subsets of T cells, such as Th17 cells and IL-17-producing $\gamma\delta$T cells. Indeed, we observed transfer of Th17-conditoned cells transiently exacerbated motor function (Figure 2d).

Activation of monocytes by Th1 cell transfer may have a role in enhanced CST sprouting and myelination after SCI, as monocyte-derived cells are required for remyelination after toxin-induced demyelination[32] or EAE.[26] It is also known that activated microglia induce neuronal differentiation[33] and are neuroprotective.[28] Specifically, M1 subtype of microglia/macrophages is considered pro-inflammatory, whereas M2 subtype is considered phagocytic and tissue-protective.[28] Indeed, we identified that microglia and macrophages were activated by transfer of Th1-conditoned cells and that M2 subtype of microglia/macrophages was upregulated (Figures 5 and 6). It should be noted that transfer of IFN-γ-producing Th1 cells that had been considered pro-inflammatory promoted upregulation of anti-inflammatory M2 subtype of microglia/macrophages after SCI.

The differentiating characteristic of our treatment from others[7,10,15] is that the transferred T cells in the present study were not immunized by CNS proteins, such as myelin basic protein or myelin oligodendrocyte glycoprotein. The fact that we observed little infiltration of the transferred Th1-conditioned cells into the injured spinal cord (data not shown) suggests that these cells did not attack the CNS.

Importantly, IL-10 expressed by Th1-conditioned cells has beneficial role in promoting functional recovery (Figure 7). Although Th2 cells also express IL-10,[30] Th2-conditioned cells did not show beneficial effects on functional recovery after SCI in our model (Figures 2a and b). Thus, expression of IL-10 from Th1-conditoned cells may contribute to maintaining the cells in an effective state *in vivo* rather than directly modulating the lesion sites.

Taken together, our successful intervention with cultured Th1-conditoned cells may shed light on a future immunomodulatory treatment for CNS injury.

Materials and Methods

Mice. C57BL/6 mice were purchased from Charles River Laboratories. All mice used in this study were housed in specific pathogen-free conditions, and were treated and cared for in accordance with the guidelines of the Osaka University pertaining to the treatment of experimental animals.

Animal model of SCI. Adult (7–9 weeks old) female C57BL/6 mice were anesthetized with sodium pentobarbital (50 mg/kg; Kyoritsu Seiyaku, Tokyo, Japan). Following dorsal laminectomy (Th.9–Th.10 level), the spinal cord was contused with a force of 60 kilodyne using an Infinite Horizon Impactor (Precision Systems & Instrumentation, Fairfax Station, VA, USA) as previously described.[34] The muscle and skin layers were then sutured. The bladder was expressed by manual abdominal pressure every day until 10 days post-injury. Food and water were provided *ad libitum*.

Adoptive transfer of cultured T cells. Spleens and lymph nodes (axillary and cervical) were collected from C57BL/6J female mice. The spleens were mechanically disrupted, washed twice, and resuspended in cold PBS. The lymph nodes were also mechanically disrupted and incubated on ice for 5 min followed by collection of the supernatant and centrifugation at 1400 r.p.m. The pellet was then suspended in cold PBS. These samples were filtrated with a 70-μm Cell Strainer (BD Biosciences, Franklin Lakes, NJ, USA) and suspended in RPMI 1640 medium (Invitrogen, Carlsbad, CA, USA) supplemented with 10% fetal bovine serum (FBS), 100 IU/ml penicillin, 100 μg/ml streptomycin, 1 μM sodium pyruvate, and 2.5 μM β-mercaptoethanol (RPMI growth medium). $CD4^+$ T cells were isolated by magnet sorting with anti-CD4 magnet beads according to the manufacturer's instructions (Miltenyi Biotec GmbH, Bergisch Gladbach, Germany). $CD4^+$ T cells were stimulated with anti-CD3ε/anti-CD28 antibodies (BD Biosciences) coated on 24-well plates (Greiner Bio One, Kremsmünster, Austria) at a concentration of 5 μg/ml each. Th1-conditioned cells were differentiated by the addition of recombinant IL-2 (25 U/ml; R&D systems, Minneapolis, MN, USA), IL-12 (10 U/ml; R&D systems), and anti-IL-4 antibodies (25% culture supernatant of hybridoma; clone HB-188; American Type Culture Collection, Manassas, VA, USA).

Th2 polarization was initiated by the addition of recombinant IL-2 (25 U/ml; R&D systems), IL-4 (100 U/ml; Peprotech, Rocky Hill, NJ, USA), and anti-IFN-γ antibodies (1% culture supernatant of hybridoma; clone HB-170; American Type Culture Collection). Th17-conditioned cells were differentiated by the addition of recombinant IL-6 (20 ng/ml; R&D systems), IL-23 (20 ng/ml; R&D systems), TGF-β1 (3 ng/ml; R&D systems), anti-IL-4 antibodies (25% culture supernatant of hybridoma; clone HB-188; American Type Culture Collection), and anti-IFN-γ antibodies (1% culture supernatant of hybridoma; clone CRL-1975; American Type Culture Collection) in the presence of recombinant IL-2 (25 U/ml; R&D systems) or anti-IL-2 antibody (10 μg/ml; R&D systems). These $CD4^+$ T cells were diluted 1 : 3 for passage on day 2, and cultured with IL-2 and IL-12 for Th1; IL-2 and IL-4 for Th2; and IL-6, IL-23, TGF-β1 with or without IL-2 for Th17 in the same concentrations as above. On day 4, these helper T cells were harvested and overlaid on Lympholyte M (Cedarlane Laboratories, Burlington, ON, Canada) and centrifuged at 1000 $\times$ *g* for 20 min. The intermediate layer was collected, washed with PBS, and resuspended in RPMI growth medium. The cells were restimulated for 3 h with anti-CD3ε and anti-CD28 antibodies (BD Biosciences) coated on 24-well plates. After restimulation with anti-CD3ε and anti-CD28 antibodies, cells were harvested and washed twice with PBS. Helper T cells (5.0×10^6 or 1.0×10^7) suspended in 500 μl PBS were injected i.p. into mice at day 4 after SCI. As a control, 500 μl PBS was injected into mice after SCI. For IL-10 neutralization, Th1 cells were incubated with anti-IL-10 antibody (eBioscience; clone: JES5-16E3) or rat IgG (eBioscience, San Diego, CA, USA) at the concentration of 10 μg/ml, and were simultaneously restimulatd with anti-CD3ε and anti-CD28 antibodies. After transfer of Th1 cells, 100 μg of anti-IL-10 antibody or rat IgG (eBioscience) was injected i.p. into mice on SCI days 5, 7, and 11.

Behavioral analysis. Hindlimb motor function was evaluated using the BMS open field locomotor test, in which scores range from 0 to 9.[35] BMS scores were recorded at days 1, 3, 7, 10, and 14 post-injury, and once weekly thereafter for a total of 11 weeks. A subset of animals was analyzed using the inclined plane task,[36] which evaluates the animal's ability to maintain body position on a board raised incrementally to increasing angles. Performance on the inclined plane correlates with the integrity of the rubrospinal tract (and other nonpyramidal pathways) after SCI.[37,38] Animals were tested at days 1, 3, 7, 10, and 14 post-injury, and once weekly thereafter for a total of 12 weeks. Mice were tested in each position, after which the angle was increased incrementally by 5°. The maximum angle at which the animal could maintain a stationary position on the board for 10 s was recorded.

Analysis of tactile sensation. To measure the threshold of hindpaw withdrawal to mechanical stimuli, we followed a reported procedure.[39] Mice were placed within an inverted glass beaker (10 cm diameter) positioned on the framework used in the grid walk test. The framework consisted of grids (1-cm^2 grids) that allowed von Frey monofilaments (SAKAI Medical Co., Ltd, Tokyo, Japan) to be applied to the plantar surface of the hindpaws. We evaluated thresholds of hindpaw withdrawal using a sequence of mechanical stimuli of increasing force. Mechanical testing was performed using 20 calibrated von Frey monofilaments that delivered approximately logarithmic incremental forces of 1.65–6.65 mg. For each group, every monofilament was applied to the hindpaw for $\sim$1 s with at least a 10-s interval between stimulus presentations. The lowest force von Frey monofilament was applied to the right, then to the left hindpaw plantar surface, and then the next higher force von Frey was administered in the same manner. A positive withdrawal response was recorded when the animal produced more than two stimulus-related withdrawals of the tested paw in three trials.

Anterograde labeling of the CST. More than 10 weeks after injury, descending CST fibers were labeled with BDA (10% in saline, 3.2 μl per cortex, MW 10 000; Invitrogen) injected under anesthesia into the left motor cortex (coordinates: 0.5–1.0 mm posterior to bregma, 0.5–1.0 mm lateral to bregma, 0.5 mm depth). For each injection, 0.2 μl BDA was delivered over a period of 30 s via a 15–20-μm inner diameter glass capillary attached to a microliter syringe (ITO). In total, we examined and compared the sprouting responses of four control and six Th1 cell-transferred mice after SCI. At 14 days after BDA injection, the animals were perfused with 4% paraformaldehyde (Wako Pure Chemical Industries, Osaka, Japan). The spinal cord was removed from the vertebral column and stored in 15% sucrose in 0.2 M phosphate buffer (PB) at 4 °C for 12 h. The spinal cord was then placed in 30% sucrose in 0.2 M PB for 24 h at 4 °C. The spinal cord was embedded in Tissue Tek OCT (Sakura Finetechnical Co. Ltd, Tokyo, Japan) and immediately frozen on dry ice at -80 °C. A series of 20-μm transverse sections were cut on a cryostat and mounted on Matsunami Adhesive Silan (MAS)-coated glass slides (Matsunami Glass, Osaka, Japan). The sections were incubated in PBS with 0.3% Triton X-100 at room temperature for 5 h, washed three times, then incubated for 2 h with Alexa Fluor 488-conjugated streptavidin (1 : 400; Invitrogen) in PBS with 0.1% Triton X-100. The sections were viewed under an inverted light microscope equipped with epifluorescence optics and a dry condenser for phase-contrast microscopy (DP70, Olympus, Tokyo, Japan). The area of positive fluorescence in the histological section was determined by using Image J software (National Institutes of Health (NIH), Bethesda, MD, USA).

Tissue preparation and histochemistry. For histochemistry, the animals were perfused with 4% paraformaldehyde, and preserved spinal cord tissues were collected. The whole spine was dissected out and post-fixed in 4% paraformaldehyde for 3 h at 4 °C. The spinal cord was removed from the vertebral column and stored for 12 h in 15% sucrose in 0.2 M PB at 4 °C. The spinal cord was then placed in 30% sucrose in 0.2 M PB for 24 h at 4 °C. The spinal cord was embedded in Tissue Tek OCT and immediately frozen on dry ice at -80 °C. A series of 20-μm transverse sections were cut on a cryostat and mounted on MAS-coated glass slides. After washing three times with PBS, all sections were blocked in PBS containing 5% BSA and 0.3% Triton X-100 for 1 h at room temperature. The sections were then incubated with primary antibodies overnight at 4 °C, washed three times with PBS, and incubated with fluorescein-conjugated secondary antibodies (1 : 500; Invitrogen) for 1 h at room temperature. Sections were then rinsed three times in PBS and mounted. For primary antibodies, we used monoclonal anti-serotonin (1 : 2000; ImmunoStar, Hudson, WI, USA) and polyclonal anti-GFAP (1 : 400; Dako, Glostrup, Denmark).

Myelin staining of spinal cord cross-sections was performed using FluoroMyelin (Invitrogen) to measure the area of myelinated nerve fibers in the white matter. The area of positive fluorescence in histological sections was determined by using Image J software (NIH). The ratios of the 5-HT-positive area 5 mm rostral to the lesion site in the Th1-transferred SCI mice to that in the PBS-treated SCI mice were calculated using pairs of the sections (PBS-treated and Th1 cell-transferred) stained on the same day to avoid decrease of the signal intensity over time.

The sections were viewed under an inverted light microscope equipped with epifluorescence optics and a dry condenser for phase-contrast microscopy (DP70, Olympus). For 5-HT immunohistochemistry of higher magnification views, samples were examined under a confocal laser-scanning microscope (FV1000, Olympus).

Preparation of leukocytes from injured spinal cords. We performed the extraction of leukocytes from the spinal cord according to a previously described procedure.[40] Firstly, mice were transcardially perfused with ice-cold PBS. The spinal cord was then dissected and suspended in Hank's Balanced Salt Solution (Invitrogen) supplemented with 3% FBS, 100 IU/ml penicillin, and 100 μg/ml streptomycin. The spinal cords were digested with collagenase D (5.0 mg/ml; Roche, Basel, Switzerland) plus 2.5 mM calcium chloride. After filtration with a 70-μm Cell Strainer (BD Biosciences), the pellet isolated by 38% Percoll centrifugation at 1500 $\times$ *g* for 20 min was collected for flow cytometry.

Staining of cell-surface and intracellular antigens. Cultured lymphocytes were stimulated with 50 ng/ml phorbol 12-myristate 13-acetate (PMA, EMD Millipore, Billerica, MA, USA) and 750 ng/ml ionomycin (EMD Millipore) for 4 h and with 10 μg/ml brefeldin A (Sigma-Aldrich, St. Louis, MO, USA) for the last 2 h. Collected leukocytes from mice spinal cords were incubated with 10 μg/ml brefeldin A (Sigma-Aldrich) for 2 h. The cells were suspended in Fixation Buffer (eBioscience), preincubated with Fc receptor block antibody (eBioscience) for 20 m, and surface stained with anti-CD4-PE (BD Biosciences), anti-CD45-Alexa647 (BioLegend, San Diego, CA, USA), anti-CD45-PE/Cy7 (BioLegend), anti-CD11b-PE, anti-CD11b-APC, anti-mouse CD86-APC, anti-mouse CD206-FITC (BioLegend). Intracellular staining was performed according to the manufacturer's protocol using anti-IL-10-PE (BioLegend) and anti-IL-6-FITC (eBioscience) antibodies with permiabilization buffer and staining buffer (eBioscience). For Arg1 staining, the permiabilized cells were incubated with mouse anti-Arg1 antibody (1 : 200; BD Biosciences) for 1 h, washed twice, and incubated with PE-conjugated anti-mouse IgG antibody (BioLegend).

Flow cytometric analysis. Flow cytometry was performed with the FACSCalibur and FACSCanto II flow cytometers (BD Biosciences) and analyzed using ProQuest and FACSDiva (BD Biosciences), and FlowJo software

(version 9.3.1; TreeStar, Inc., Ashland, OR, USA). Specificity of the signals of antibodies against specific antigens was determined by performing control experiments using isotype-matched immunoglobulins (BioLegend).

Enzyme-linked immunosorbent assay. Th1, Th2, and Th17 (cultured with anti-IL-2 antibody) cells were prepared as described above. Three hours after restimulation with anti-CD3ε/anti-CD28 antibodies, the cells were centrifuged and their supernatants were collected and stored at − 80 °C until use. Concentrations of NT-3, GDNF, BDNF in the supernatants of each cell were analyzed using the ELISA kits according to the manufacturer's protocol (Emax Immunoassay System (Promega, Fitchburg, WI, USA) for NT-3, GDNF, and BDNF. Absorbance values were read at 450 nm on a plate reader (SpectraMax M2; Molecular Devices, Sunnyvale, CA, USA).

Statistical analysis. All values are expressed as mean ± S.E.M. We analyzed motor function scores using two-way ANOVA with repeated measures, Bonferroni post-test for 2–4 groups. Quantified histological data were analyzed by the Mann–Whitney *U* test. However, for Figure 3f, the result was analyzed by paired Student's *t* test. Student's *t* test was used to analyze the quantified data with flow cytometry. For all other data, we used one-way ANOVA with Dunnett post-test collection for comparison of 3–4 groups. Values of $P<0.05$ were considered statistically significant.

Conflict of Interest

The authors declare no conflict of interest.

Acknowledgements. We thank Drs. T Nakayama, M Yamashita and M Kuwahara at Chiba University, and Drs. M Murakami, D Kamimura and H Okuyama at Osaka University, for their technical advice on T-cell culture; Drs. K Morimoto and S Lee at Osaka University for their help in histological assessment.

1. Taoka Y, Okajima K, Uchiba M, Murakami K, Kushimoto S, Johno M *et al.* Role of neutrophils in spinal cord injury in the rat. *Neuroscience* 1997; **79**: 1177–1182.
2. Profyris C, Cheema SS, Zang D, Azari MF, Boyle K, Petratos S. Degenerative and regenerative mechanisms governing spinal cord injury. *Neurobiol Dis* 2004; **15**: 415–436.
3. Potas JR, Zheng Y, Moussa C, Venn M, Gorrie CA, Deng C *et al.* Augmented locomotor recovery after spinal cord injury in the athymic nude rat. *J Neurotrauma* 2006; **23**: 660–673.
4. Park E, Velumian AA, Fehlings MG. The role of excitotoxicity in secondary mechanisms of spinal cord injury: a review with an emphasis on the implications for white matter degeneration. *J Neurotrauma* 2004; **21**: 754–774.
5. Moalem G, Leibowitz-Amit R, Yoles E, Mor F, Cohen IR, Schwartz M. Autoimmune T cells protect neurons from secondary degeneration after central nervous system axotomy. *Nat Med* 1999; **5**: 49–55.
6. Hammarberg H, Lidman O, Lundberg C, Eltayeb SY, Gielen AW, Muhallab S *et al.* Neuroprotection by encephalomyelitis: rescue of mechanically injured neurons and neurotrophin production by CNS-infiltrating T and natural killer cells. *J Neurosci* 2000; **20**: 5283–5291.
7. Hauben E, Butovsky O, Nevo U, Yoles E, Moalem G, Agranov E *et al.* Passive or active immunization with myelin basic protein promotes recovery from spinal cord contusion. *J Neurosci* 2000; **20**: 6421–6430.
8. Yoles E, Hauben E, Palgi O, Agranov E, Gothilf A, Cohen A *et al.* Protective autoimmunity is a physiological response to CNS trauma. *J Neurosci* 2001; **21**: 3740–3748.
9. Hofstetter HH, Sewell DL, Liu F, Sandor M, Forsthuber T, Lehmann PV *et al.* Autoreactive T cells promote post-traumatic healing in the central nervous system. *J Neuroimmunol* 2003; **134**: 25–34.
10. Ziv Y, Ron N, Butovsky O, Landa G, Sudai E, Greenberg N *et al.* Immune cells contribute to the maintenance of neurogenesis and spatial learning abilities in adulthood. *Nat Neurosci* 2006; **9**: 268–275.
11. Beers DR, Henkel JS, Zhao W, Wang J, Appel SH. CD4+ T cells support glial neuroprotection, slow disease progression, and modify glial morphology in an animal model of inherited ALS. *Proc Natl Acad Sci USA* 2008; **105**: 15558–15563.
12. Chiu IM, Chen A, Zheng Y, Kosaras B, Tsiftsoglou SA, Vartanian TK *et al.* T lymphocytes potentiate endogenous neuroprotective inflammation in a mouse model of ALS. *Proc Natl Acad Sci USA* 2008; **105**: 17913–17918.
13. Gimsa U, Peter SV, Lehmann K, Bechmann I, Nitsch R. Axonal damage induced by invading T cells in organotypic central nervous system tissue in vitro: involvement of microglial cells. *Brain Pathol* 2000; **10**: 365–377.
14. Fee D, Crumbaugh A, Jacques T, Herdrich B, Sewell D, Auerbach D *et al.* Activated/effector CD4+ T cells exacerbate acute damage in the central nervous system following traumatic injury. *J Neuroimmunol* 2003; **136**: 54–66.
15. Jones TB, Ankeny DP, Guan Z, McGaughy V, Fisher LC, Basso DM *et al.* Passive or active immunization with myelin basic protein impairs neurological function and exacerbates neuropathology after spinal cord injury in rats. *J Neurosci* 2004; **24**: 3752–3761.
16. Shichita T, Sugiyama Y, Ooboshi H, Sugimori H, Nakagawa R, Takada I *et al.* Pivotal role of cerebral interleukin-17-producing gammadeltaT cells in the delayed phase of ischemic brain injury. *Nat Med* 2009; **15**: 946–950.
17. Kebir H, Kreymborg K, Ifergan I, Dodelet-Devillers A, Cayrol R, Bernard M *et al.* Human TH17 lymphocytes promote blood-brain barrier disruption and central nervous system inflammation. *Nat Med* 2007; **13**: 1173–1175.
18. Hendrix S, Nitsch R. The role of T helper cells in neuroprotection and regeneration. *J Neuroimmunol* 2007; **184**: 100–112.
19. Ishii H, Kubo T, Kumanogoh A, Yamashita T. Th1 cells promote neurite outgrowth from cortical neurons via a mechanism dependent on semaphorins. *Biochem Biophys Res Commun* 2010; **402**: 168–172.
20. Zhang P, Smith R, Chapkin RS, McMurray DN. Dietary (n-3) polyunsaturated fatty acids modulate murine Th1/Th2 balance toward the Th2 pole by suppression of Th1 development. *J Nutr* 2005; **135**: 1745–1751.
21. O'Garra A, Murphy K. Role of cytokines in determining T-lymphocyte function. *Curr Opin Immunol* 1994; **6**: 458–466.
22. Wurster AL, Rodgers VL, Satoskar AR, Whitters MJ, Young DA, Collins M *et al.* Interleukin 21 is a T helper (Th) cell 2 cytokine that specifically inhibits the differentiation of naive Th cells into interferon gamma-producing Th1 cells. *J Exp Med* 2002; **196**: 969–977.
23. Jäger A, Dardalhon V, Sobel RA, Bettelli E, Kuchroo VK *et al.* Th1, Th17, and Th9 effector cells induce experimental autoimmune encephalomyelitis with different pathological phenotypes. *J Immunol* 2009; **183**: 7169–7177.
24. Laurence A, Tato CM, Davidson TS, Kanno Y, Chen Z, Yao Z *et al.* Interleukin-2 signaling via STAT5 constrains T helper 17 cell generation. *Immunity* 2007; **26**: 371–381.
25. Kim JE, Liu BP, Park JH, Strittmatter SM. Nogo-66 receptor prevents raphespinal and rubrospinal axon regeneration and limits functional recovery from spinal cord injury. *Neuron* 2004; **44**: 439–451.
26. Butovsky O, Landa G, Kunis G, Ziv Y, Avidan H, Greenberg N *et al.* Induction and blockage of oligodendrogenesis by differently activated microglia in an animal model of multiple sclerosis. *J Clin Invest* 2006; **116**: 905–915.
27. Shechter R, London A, Varol C, Raposo C, Cusimano M, Yovel G *et al.* Infiltrating blood-derived macrophages are vital cells playing an anti-inflammatory role in recovery from spinal cord injury in mice. *PLoS Med* 2009; **6**: e1000113.
28. Kigerl KA, Gensel JC, Ankeny DP, Alexander JK, Donnelly DJ, Popovich PG. Identification of two distinct macrophage subsets with divergent effects causing either neurotoxicity or regeneration in the injured mouse spinal cord. *J Neurosci* 2009; **29**: 13435–13444.
29. David S, Kroner A. Repertoire of microglial and macrophage responses after spinal cord injury. *Nat Rev Neurosci* 2011; **12**: 388–399.
30. Saraiva M, Christensen JR, Veldhoen M, Murphy TL, Murphy KM, O'Garra A. Interleukin-10 production by Th1 cells requires interleukin-12-induced STAT4 transcription factor and ERK MAP kinase activation by high antigen dose. *Immunity* 2007; **31**: 209–219.
31. Rossignol S, Schwab M, Schwartz M, Fehlings MG. Spinal cord injury: time to move? *J Neurosci* 2007; **27**: 11782–11792.
32. Kotter MR, Setzu A, Sim FJ, Van Rooijen N, Franklin RJ. Macrophage depletion impairs oligodendrocyte remyelination following lysolecithin-induced demyelination. *Glia* 2001; **35**: 204–212.
33. Butovsky O, Ziv Y, Schwartz A, Landa G, Talpalar AE, Pluchino S. Microglia activated by IL-4 or IFN-gamma differentially induce neurogenesis and oligodendrogenesis from adult stem/progenitor cells. *Mol Cell Neurosci* 2006; **31**: 149–160.
34. Engesser-Cesar C, Anderson AJ, Basso DM, Edgerton VR, Cotman CW. Voluntary wheel running improves recovery from a moderate spinal cord injury. *J Neurotrauma* 2005; **22**: 157–171.
35. Basso DM, Fisher LC, Anderson AJ, Jakeman LB, McTigue DM, Popovich PG. Basso Mouse Scale for locomotion detects differences in recovery after spinal cord injury in five common mouse strains. *J Neurotrauma* 2006; **23**: 635–659.
36. Rivlin AS, Tator CH. Objective clinical assessment of motor function after experimental spinal cord injury in the rat. *J Neurosurg* 1977; **47**: 577–581.
37. Fehlings MG, Tator CH. The relationships among the severity of spinal cord injury, residual neurological function, axon counts, and counts of retrogradely labeled neurons after experimental spinal cord injury. *Exp Neurol* 1995; **132**: 220–228.
38. Sundberg LM, Herrera JJ, Narayana PA. In vivo longitudinal MRI and behavioral studies in experimental spinal cord injury. *J Neurotrauma* 2010; **10**: 1753–1767.
39. Fuchs PN, Roza C, Sora I, Uhl G, Raja SN. Characterization of mechanical withdrawal responses and effects of mu-, delta- and kappa-opioid agonists in normal and mu-opioid receptor knockout mice. *Brain Res* 1999; **821**: 480–486.
40. Serada S, Fujimoto M, Mihara M, Koike N, Ohsugi Y, Nomura S *et al.* IL-6 blockade inhibits the induction of myelin antigen-specific Th17 cells and Th1 cells in experimental autoimmune encephalomyelitis. *Proc Natl Acad Sci USA* 2008; **105**: 9041–9046.

Tumor Biol. (2012) 33:1141–1149
DOI 10.1007/s13277-012-0356-9

RESEARCH ARTICLE

Serum HE4 as a diagnostic and prognostic marker for lung cancer

Kota Iwahori · Hidekazu Suzuki · Yoshiro Kishi · Yoshihiro Fujii · Rie Uehara · Norio Okamoto · Masashi Kobayashi · Tomonori Hirashima · Ichiro Kawase · Tetsuji Naka

Received: 19 December 2011 / Accepted: 9 February 2012 / Published online: 29 February 2012

Abstract We evaluated the diagnostic and prognostic efficacy of human epididymis protein 4 (HE4) for lung cancer patients by using our novel enzyme-linked immunosorbent assay (ELISA) system. We measured serum HE4 levels of cancer patients including 49 lung cancer and 18 ovarian cancer patients. Furthermore, we evaluated the relationship between serum HE4 levels and overall survival after chemotherapy of 24 lung cancer patients. Serum HE4 levels were significantly higher for non-small, small cell lung cancer and ovarian cancer patients than for healthy controls. The area under the receiver operating characteristic curve (AUC) was calculated for differentiation of lung cancer patients and healthy controls. AUC for serum HE4 was 0.988 for differentiating lung cancer patients from healthy controls, with a cutoff value of 6.56 ng/ml (sensitivity= 89.8%, specificity=100%). Serum HE4 levels were elevated in 36/40 (90.0%) non-small cell lung cancer patients, 8/9 (88.9%) small cell lung cancer patients and 8/18 (44.4%) ovarian cancer patients. High levels of serum HE4 (>15 ng/ml) after chemotherapy were significantly correlated with worse overall survival after the treatment. These findings suggest that serum HE4 is a potential diagnostic and prognostic marker for lung cancer patients.

Keywords HE4 · Tumor marker · ELISA · Lung cancer · Chemotherapy

K. Iwahori · T. Naka (✉)
Laboratory for Immune Signal,
National Institute of Biomedical Innovation,
7-6-8 Saito-Asagi,
Ibaraki, Osaka 567-0085, Japan
e-mail: tnaka@nibio.go.jp

K. Iwahori
Department of Respiratory Medicine, Allergy, and Rheumatic Diseases, Osaka University Graduate School of Medicine,
2-2 Yamada-oka,
Suita, Osaka 565-0871, Japan

H. Suzuki · N. Okamoto · M. Kobayashi · T. Hirashima · I. Kawase
Department of Thoracic Malignancy, Osaka Prefectural Medical Center for Respiratory and Allergic Diseases,
3-7-1 Habikino,
Habikino, Osaka 583-8588, Japan

Y. Kishi · Y. Fujii · R. Uehara
Medical & Biological Laboratories, Co., Ltd.,
4-5-3, Sakae, Naka-ku,
Nagoya 460-0008, Japan

Introduction

Lung cancer is the leading cause of death in adult men in Europe, the United States, and Japan. In 2010, approximately 157,300 Americans died of lung cancer from among 569,490 cancer deaths [1]. The exceptionally high mortality rate of lung cancer is, in part, due to the fact that lung cancer is often diagnosed at a late stage when the prognosis is usually poor, and early detection continues to be an elusive goal. For patients with advanced stage disease, modest but real improvements in overall survival and quality of life have been achieved with systemic chemotherapy [2]. However, the determination of efficacy of chemotherapy during the early phase of treatment is difficult to achieve. The decision whether to continue or to stop chemotherapy is traditionally guided by imaging-based tumor response evaluation, which is regarded as a surrogate marker of clinical benefit. Assessment by structural imaging has known limitations and also may have a poor correlation with pathologic response in non-small cell lung cancer [3]. On the other

hand, tumor markers that are currently available for lung cancer such as carcinoembryonic antigen (CEA), serum cytokeratin 19 fragment (CYFRA 21-1) and progastrin-releasing peptide (pro-GRP) are not satisfactory for diagnosis at an early stage or for monitoring the disease because of their relatively low sensitivity and specificity in detecting the presence of cancer cells [4–6]. Therefore, the identification of novel diagnostic and prognostic biomarkers for treatment response is eagerly desired.

Human epididymis protein 4 (HE4) was first identified in the epithelium of the distal epididymis and originally predicted to be a protease inhibitor involved in sperm maturation [7, 8]. Regarding malignant neoplasms, gene expression profiling studies have identified upregulation of HE4 in ovarian cancer [9–14], and several studies have shown HE4 protein expression in ovarian cancer, providing the opportunity for its application in histopathologic diagnosis [15–18]. Recent studies have revealed elevated HE4 protein levels in serum from ovarian cancer patients [19]. Moreover, HE4 protein expression was analyzed in other neoplasms including lung cancer [20, 21]. In this study, we developed novel enzyme-linked immunosorbent assay (ELISA) system to detect serum HE4, and by using this system, we showed that HE4 has potential for diagnostic marker of lung cancer. Specifically, we found that HE4 level after chemotherapy is strongly correlated with survival after the treatment.

Materials and methods

Patients and controls for measurement of HE4

Serum samples were collected from 49 consecutive patients with lung cancer (33 with adenocarcinoma, six with squamous cell carcinoma, one with large cell carcinoma and nine with small cell carcinoma), 18 with ovarian cancer, 10 with gastric cancer and eight with colon cancer. For control, we used 37 healthy adults (Table 1). The age range in 37 healthy control subjects was between 24 and 65 years. The age range in 49 lung cancer patients was between 40 and 78 years. We obtained written and oral informed consent from all participants. This study was approved by our institutional review board (IRB).

Patients for evaluation of chemotherapy

This prospective, IRB-approved study included 24 patients enrolled between 28 April 2008 and 26 August 2008. Patient characteristics are presented in Table 2. The median age was 69 years (45–76 years). All patients received chemotherapies. Specific regimens are presented in Table 2. Computed tomography (CT) scans were performed after 2 cycles of chemotherapy or 1 month of gefitinib/erlotnib therapy. All patients had measurable disease. Response categories were defined according to the Response Evaluation Criteria in Solid Tumors (RECIST) as complete response (CR), partial response (PR), stable disease (SD) and progressive disease (PD).

Cell lines

Nonsmall cell lung cancer cell lines A549, NCI-H1793, LU61, PC14, PC14PE6, PC9, SKLU1 and SKMES2; breast cancer cell line MCF7; colon cancer cell lines LOVO and WiDr; gastric cancer cell lines GC1Y, GT3TKB, HGC27, KATO3, MKN45 and OCUM1; pancreatic cancer cell line Miapaca2; prostate cancer cell lines 22Rv1 and PC3; and bladder cancer cell line T24 were cultured in DMEM medium (Sigma, St Louis, MO) supplemented with 10% fetal bovine serum (Equitech Bio Inc., Kerrville, TX). Non-small cell lung cancer cell line A427 was cultured in E-MEM medium (Sigma) supplemented with 10% fetal bovine serum. Non-small cell lung cancer cell lines NCI-H226, NCI-H358, NCI-H520, NCI-H522, NCI-H596, NCI-H2170, LC174, LC319 and ChagoK1; small cell lung cancer cell line DMS114; gastric cancer cell lines SCH, MKN74 and MKN1; pancreatic cancer cell lines KLM1, PK59 and PK1; and breast cancer cell line T47D were cultured in RPMI (Sigma) supplemented with 10% fetal bovine serum.

Table 1 Serum concentrations of HE4 in cancer patients and controls

Diagnosis	Number of study participants	HE4 (ng/ml)			Positive ratio (%)
		Mean (SD)	Median	Range	(Cutoff 6.56 ng/ml)
Lung cancer	49	14.0 (9.5)	11.4	4.3–63.4	89.8
NSCLC	40	13.3 (6.5)	11.4	4.3–30.7	90.0
SCLC	9	17.3 (18.1)	11.4	5.5–63.4	88.9
Ovarian cancer	18	10.9 (13.6)	6.1	2.0–60.2	44.4
Gastric cancer	10	7.2 (4.4)	7.1	2.1–17.4	60.0
Colorectal cancer	8	7.7 (3.5)	7.1	3.0–12.2	62.5
Normal	37	2.7 (1.2)	2.4	1.3–5.8	

Table 2 Patient characteristics

Characteristics	Number of patients
Gender	
Males/females	16/8
Age (years)	
<71/>71	13/11
Stage	
3A/3B/4	4/5/15
Tumor histology	
Adenocarcinoma	15
Squamous	4
Unclassified NSCLC	1
Small	4
Chemotherapy	
NSCLC	
Carboplatin + paclitaxel	5
Vinorelbine	3
Irinotecan	3
Cisplatin + gemcitabine	2
Gefitinib	2
Erlotinib	2
Carboplatin + gemcitabine	1
Cisplatin + vinorelbine	1
Gemcitabine	1
SCLC	
Carboplatin + etoposide	2
Cisplatin + etoposide	1
Cisplatin + irinotecan	1
Clinical response	
NSCLC	
CR/PR/SD/PD	0/5/10/5
SCLC	
CR/PR/SD/PD	0/3/1/0

Culture supernatants were collected at 5 to 6 days after cultivation and stored at 4°C until test.

Antigen preparation

Recombinant human HE4 protein was produced by amplifying the part coding for amino acids 1–124 from the cDNA encoding the transcript for human HE4 (Genbank accession no. NM_006103) with DNA polymerase (recombinant Taq polymerase; Takara Bio Inc., Shiga, Japan) and using the primers 5′-CGGGATCCGAGAAGACTGGCGTGTGCCCCG-3′ and 5′-TTTAAAGCGGCCGCTCAGAAATTGGGAGTGACA CAGG-3′. The amplified DNA was inserted into the *Bam*HI/*Not*I site of a mammalian expression plasmid DNA vector pSecTag2/Myc-His (Invitrogen, Carlsbad, CA) and transfected into HEK 293 T cells by lipofection (Lipofectamine 2000; Invitrogen). The culture supernatant of the transfectant was recovered at 5 days after lipofection and applied to a TALON resin to purify the secreted His-tagged proteins according to the manufacturer's instructions (Takara). The purified HE4 protein thus obtained was dialyzed with 4.0 l of PBS twice and kept frozen at −80°C until use as an immunogen or as a standard polypeptide for sandwich ELISA. Purity of the recombinant HE4 was confirmed by Coomassie Brilliant Blue (CBB) staining after electrophoresis under reduced condition (Fig. 1a).

Membrane-bound form of HE4 was constructed by molecular fusion together with the transmembrane region of a type I cell surface protein HIDE1 (accession number: A8MVS5) as briefly described below. Membrane-bound form of HE4 was produced by amplifying the part coding for amino acids 1–125 and 114–164 from the cDNAs of HE4 gene and HIDE1 gene, respectively, and both amplified DNAs were inserted into the *Xba*I site of pcDNA3.1/myc-His. *IRES-GFP* gene (Cell Biolabs, Inc., San Diego, CA) was then inserted into the *Pme*I site of the same plasmid DNA. The plasmid DNA was transfected into HEK 293 T cells, and GFP-positive cells were accounted for the cells expressing membrane bounded HE4.

Immunogen to develop a polyclonal antibody to human HE4 was prepared as follows. The part coding for amino acids 31–124 of the HE4 cDNA was ligated to the *Eco*RI/*Xho*I site of a bacterial expression vector pET28a (Novagen, Madison, WI). BL21 (DE3) competent cell (Takara) was transformed with the pET28a plasmid and cultured in LB medium. After induction of expression of HE4 protein using IPTG, the bacteria was collected and lysed with PBS containing 8 M urea, 1% NP-40, 0.5 mM PMSF and protease inhibitor cocktail (Sigma, St. Louis, MO). After centrifugation at 13,000*g* for 15 min, the supernatant containing His-tagged HE4 protein was loaded on a TALON resin, and the recombinant HE4 was eluted from the resin with 200 mM imidazole solution according to the manufacturer's instructions (Takara).

Antibody generation

To generate monoclonal antibodies against human HE4, 4-week-old BALB/c mice were immunized intraperitoneally with the recombinant HE4 produced from 293 T transfectant on days 0, 7, 14 and 16 (10 μg/shot). Following the last immunization, lymphocytes of the spleen were collected and fused with P3U1 myeloma cells in a 50% polyethylene glycol 4000 solution (Wako, Osaka, Japan) on day 18. The fused cells were plated on 96-well plates with RPMI-1640 medium containing 15% fetal calf serum (Equitech-Bio), penicillin/streptomycin (Invitrogen, Carlsbad, CA) and HAT solution (Invitrogen). After 10 days of incubation at 37°C with 5% CO_2 in a humidified environment, culture supernatants were collected and screened for their ability to bind to the immunogen by ELISA using recombinant HE4. Selected positive hybridoma colonies were expanded and

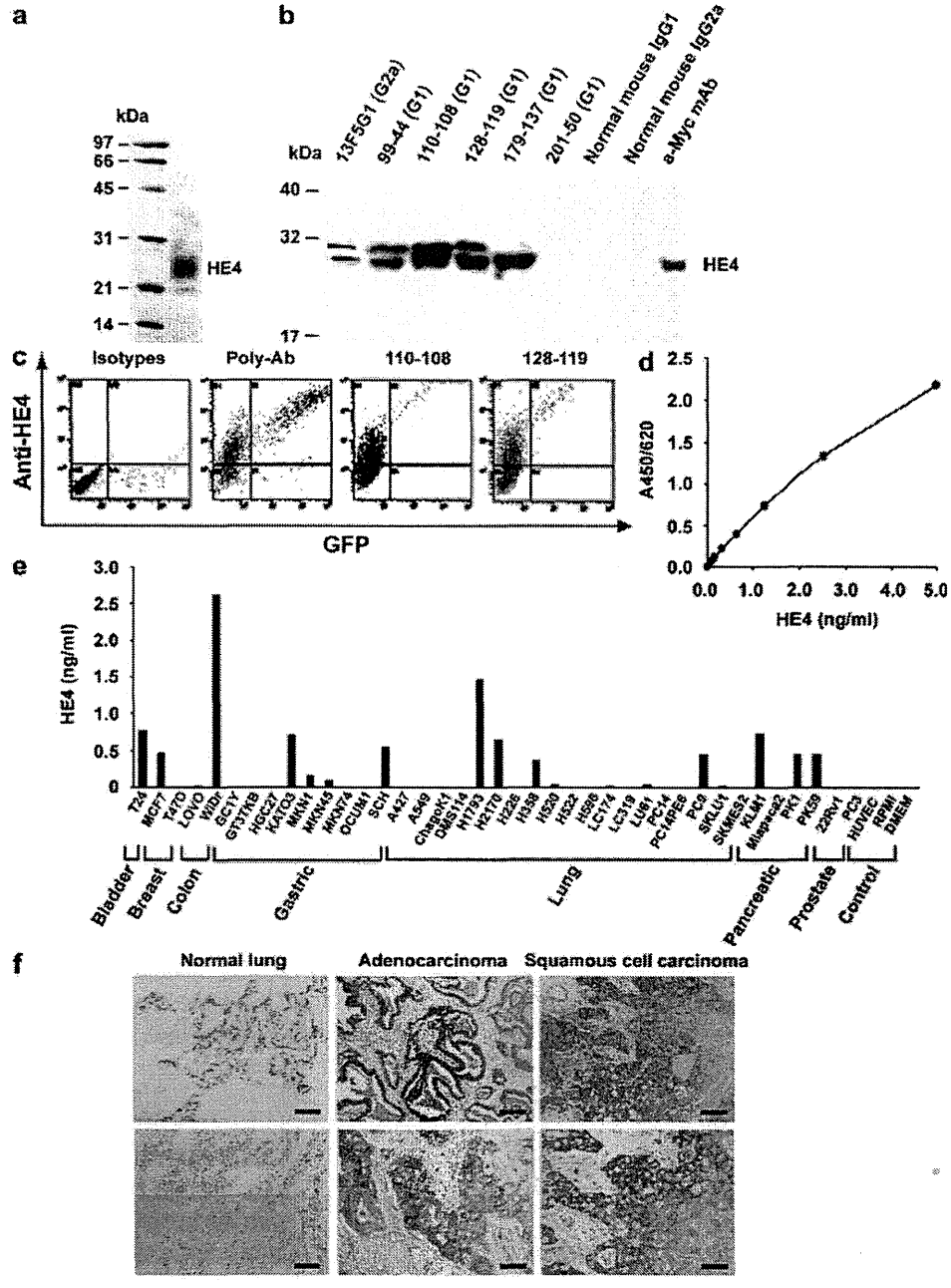

Fig. 1 **a** Purity of the prepared recombinant HE4 proteins for immunization. Proteins were electrophoresed under reduced condition and stained with Coomassie Brilliant Blue. **b** Reactivity of anti-HE4 antibodies to recombinant HE4 protein. Anti-HE4 antibodies were used for immunoprecipitation. Recovered proteins were separated by SDS-PAGE and electrotransferred to polyvinylidenefluoride (PVDF) membranes. Membranes were probed with anti-myc antibody for myc-His tagged HE4. Recombinant HE4 protein was applied for positive control. **c** Expression of HE4 on the surface of HE4-transfected 293 T cells. 293 T cells were incubated with anti-HE4 antibodies (110-108 and 128-119) or an isotype-matched control antibody and followed by PE-conjugate anti mouse IgG. Antigen expression was detected by flow cytometry. **d** Standard curves for HE4 in sandwich ELISA. ELISA displaying the mean absorbance values from indicated concentrations of recombinant proteins. **e** HE4 levels in the supernatants of cell lines measured by specific ELISA systems. **f** Immunohistochemical analysis of HE4 in lung cancer tissue. *Scale bar upper panels* 100 μm, *scale bar lower panels* 50 μm

subcloned by limiting dilution. An isostrip kit (Hoffmann-La Roche, Basel, Switzerland) was used for antibody isotype determination according to the manufacturer's instructions. Antibody purification was carried out with protein A affinity chromatography (GE Healthcare, Buckinghamshire, UK). Following a competition assay for the immunogen among the clones thus obtained (data not shown), clone 110-108 (IgG1) and clone 128-119 (IgG1) were selected to construct a sandwich ELISA for the detection of HE4.

Polyclonal antibody to recombinant human HE4 was prepared by injecting Japanese white rabbits (Kitayama Labs, Nagano, Japan) with purified HE4 (100 μg/injection) from *E. coli* subcutaneously in complete Freund's adjuvant followed by subsequent boosts in incomplete Freund's (Sigma). The serum was collected and IgG-purified with Protein G Sepharose (GE Healthcare).

Flow cytometry

At 24 h after transfection of the plasmid DNA-encoding membrane-binding HE4 into 293 T cells, the transfectant was treated with PBS containing 5 mM EDTA for 3 min to

detach from the culture dish, washed with PBS twice and incubated with 1 μg/ml of anti-HE4 antibodies or isotype-matched control for 30 min at 4°C in PBS containing 0.5% BSA and 2 mM EDTA. Following washing with the above buffer twice, PE conjugate antimouse IgG (MBL, Nagoya, Japan) for monoclonal antibody and PE-conjugated anti-rabbit polyclonal antibody (MBL) were added and further incubated for 30 min at 4°C. All flow cytometry was performed on Cytomics FC500 (Beckman Coulter, Fullerton, CA).

Immunoprecipitation and Western blot

The reactivity of anti-HE4 antibodies to recombinant HE4 protein was confirmed by immunoprecipitation. Fifteen microliters of Protein G sepharose suspended in PBS containing 0.01% BSA (Sigma) was incubated with 5 μg of anti-HE4 antibodies for 2 h at 4°C with gentle rocking. During this step, 250 ng of the recombinant myc-His-tagged HE4 protein was incubated with Protein G beads for 30 min at 4°C with shaking to preclear the samples. The Protein G Sepharose incubated with the antibodies were centrifuged at 1,000*g* for 2 min and washed with PBS three times. Then, the precleared samples were added to the tube containing the washed Protein G sepharose and rotated overnight at 4°C. After the incubation, the beads were washed with PBS three times and boiled in 25 μl of 2× Laemmli's SDS sample buffer for 5 min. Proteins (20 μl of sample per lane) were separated by sodium dodecylsulfate-polyacrylamide gel electrophoresis (SDS-PAGE) on a 12.5% polyacrylamide gel and electrotransfered to a polyvinylidenefluoride (PVDF) membrane. The membrane blocked with 5% nonfat milk in PBS containing 0.05% Tween 20 (blocking buffer) was incubated with 1.0 μg/ml mouse monoclonal anti-Myc antibody (MBL) to react with the precipitated Myc-His-tagged HE4 for 1 h at room temperature. After three washes with PBS containing 0.05% Tween 20, the membrane was incubated with a horseradish peroxidase (HRP)-conjugated antimouse IgG (MBL) diluted 1:5,000 with the blocking buffer. Chemiluminescence was developed according to the manufacturer's procedure (ECL; GE Healthcare).

Sandwich ELISA

The concentration of HE4 in culture media of cancer cell lines and donor sera was measured by a HE4-specific sandwich ELISA constructed as follows: 96-well microtiter plates (Nalge Nunc International Corp., Rochester, NY) were coated with the capturing antibody clone 110-108 with carbonate buffer at 4°C overnight. The plates were blocked with 200 μl PBS containing 1.0% BSA for 2 h and then incubated for 1 h with culture media diluted to 1:2 with sample diluent which consists of PBS containing 1.0% BSA and 0.1% Tween 20 or serum samples diluted to 1:10 with the same diluent and HRP-conjugated antibody 128-119 diluted to 1:140,000 with PBS containing BSA. After washing the plates with PBS containing Tween20, 100 μl/well TMB (Moss Inc., Pasadena, MD) was added, and the plates were incubated for 30 min at room temperature. The color development was stopped by the addition of H_2SO_4. Color intensity was determined at a wavelength of 450 nm with a reference wavelength of 620 nm. Analyte concentrations were calculated by referring to the standard curve using serial diluted recombinant HE4 (Fig. 1d).

Immunohistochemistry

Paraffin-embedded cancer tissue slices or noncancer tissue slices derived from lung cancer patients (adenocarcinoma and squamous cell carcinoma) were purchased from Outdo, Shanghai, China. The tissue slices were deparaffinized by treatment with xylene for 5 min three times, 100% ethanol for 5 min twice, 90% ethanol for 5 min once, 80% ethanol for 5 min once, 70% ethanol for 5 min once and PBS for 5 min three times. Subsequently, for an antigen retrieval, the specimens were immersed in a citrate buffer and heated by microwave for 10 min twice. In order to inactive the endogenous peroxidase activity, the specimens were then treated with PBS containing a 3% hydrogen peroxide solution at room temperature for 10 min. After washing with PBS twice, the specimens were blocked with blocking buffer and incubated with a blocking buffer containing 1 μg/ml of polyclonal HE4 antibody for 1 h at room temperature. After washing with PBS twice, the specimens were incubated with HRP-conjugated second antibody (EnVision Dual Link, Dako, Denmark) for 1 h at room temperature. Subsequently, the specimens were washed with PBS twice and allowed to react with a DAB chromogen (Dako) for 10 min at room temperature. The reaction was stopped by washing with water. After counterstaining with hematoxylene, the tissue slices were dehydrated with ethanol and xylene and made into specimens using a mounting medium (Matsunami Glass, Osaka, Japan).

Statistical analysis

To test for statistically significant differences between two groups, an unpaired Student's *t*-test was used. For comparisons among three or more groups, the values were analyzed by one-way ANOVA followed by Scheffe's post hoc comparisons. Differences were considered significant at $P<0.05$. For drawing of receiver operating characteristic (ROC) curves and estimation of the area under the ROC curve (AUC) statistics software SPBS (Comworks, Saitama, Japan) was used to quantify the ability to differentiate between

healthy volunteers and patients with lung cancer. Analyses of the prognostic impact of serum HE4 levels on survival from response evaluation to death or last follow-up used the Kaplan–Meier method and logrank test.

Results

Generation of ELISA specific for HE4

To generate monoclonal antibodies that specifically react with HE4, recombinant HE4 protein corresponding to the amino acids 1–124 of the transcript for human HE4 was produced by 293 T transfectants (Fig. 1a) and immunized to BALB/c mice. Supernatants of obtained hybridomas were tested for binding activity to microplates coated with immunizing antigen and further examined by a competition assay for the immunogen (data not shown). The specific reactivities of selected clone 13F5G1, 99-44, 110-108, 128-119, 179-137 and 201-50 to HE4 were checked by immunoprecipitation using myc-His-tagged recombinant HE4 (Fig. 1b). The specificity of 110-108 and 128-119 to HE4 was tested using the 293 T transfectant-expressing HE4 by flowcytometory. Clones 110-108 and 128-119 detected the antigen on the cell surface of 293 T transfectant (Fig. 1c). A sandwich ELISA for HE4 was constructed using the anti-HE4 antibodies 110-108 and 128-119. The standard curve using purified recombinant HE4 is shown in Fig. 1d. The HE4 sandwich ELISA detected the antigen in the culture supernatant of the various types of cancer cell lines (Fig. 1e). We investigated immunohistochemical staining of lung cancer tissue using anti-HE4 antibody. HE4 expression was detected in lung cancer tissues but not in normal lung tissues. We compared HE4 staining between adenocarcinoma and squamous cell carcinoma lung tissue samples but could not detect significant differences in staining intensity. Furthermore, we could not find a correlation between differentiation and HE4 staining of lung cancer tissues. Strong HE4 staining was

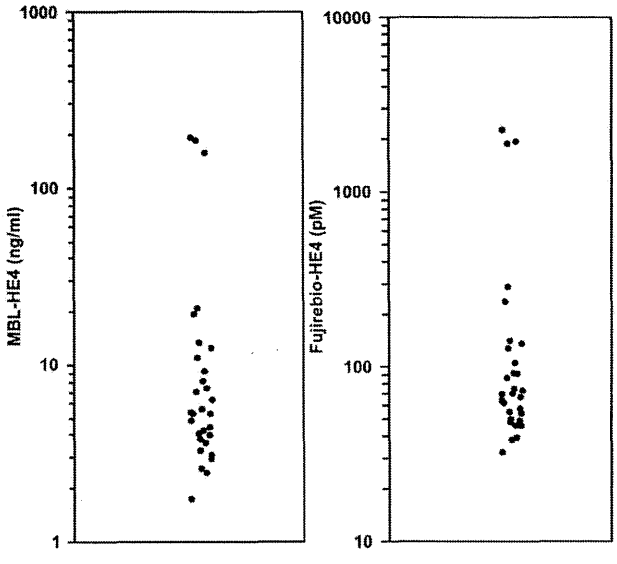

Fig. 2 HE4 levels in sera of ovarian cancer patients. HE4 levels determined by our ELISA system (*left*) and Fujirebio commercial ELISA kit (*right*). Each *dot* represents one patient

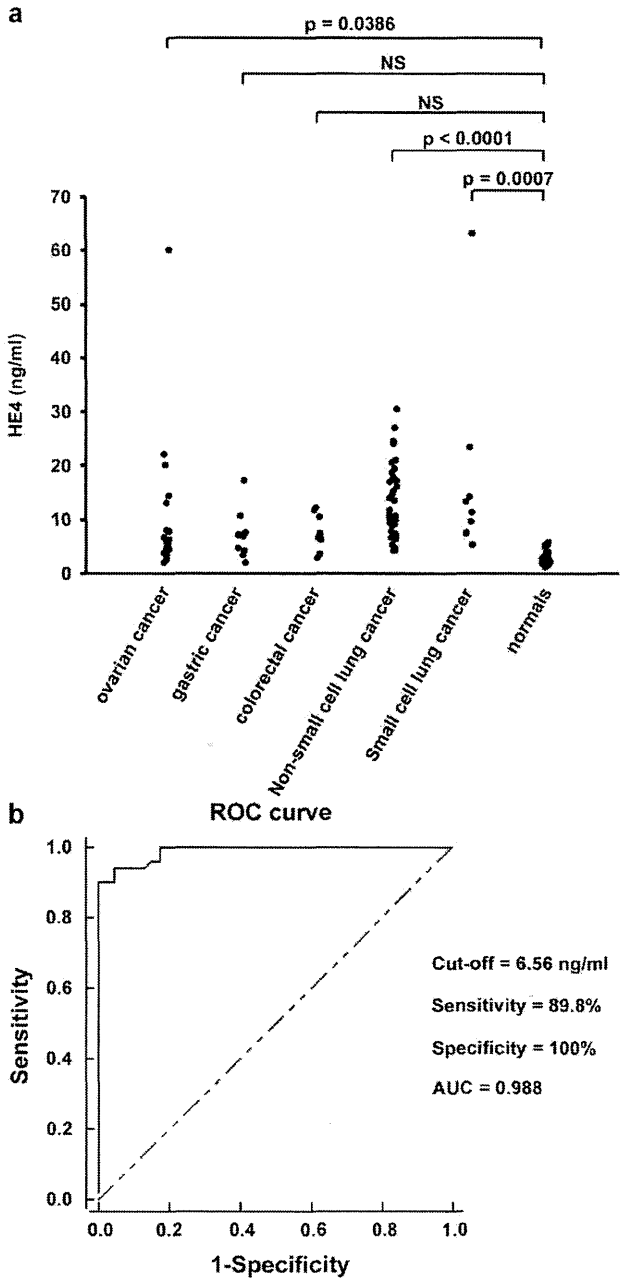

Fig. 3 **a** HE4 levels in the sera of cancer patients and normal controls. Each dot represents one patient. *NS* no significant. **b** Receiver operating characteristic (ROC) curves for HE4 for differentiation between lung cancer and healthy volunteers. The tables show the best statistical cutoff values for HE4 with pairs of sensitivity and specificity

Table 3 Pre- and post-treatment HE4 in lung cancer patients

Clinical response	Number of patients	Pre-treatment HE4 (ng/ml)			Post-treatment HE4 (ng/ml)		
		Mean (SD)	Median	Range	Mean (SD)	Median	Range
PR	8	23.0 (26.3)	14.2	8.3–86.5	12.6 (2.8)	12.9	8.2–16.1
SD	11	22.2 (32.3)	11.4	3.7–116.6	28.3 (44.4)	14.2	3.7–158.1
PD	5	21.3 (7.3)	22.8	9.3–28.1	23.8 (5.9)	25.9	14.2–29.1

detected in cytoplasmic and plasma membrane areas but not in nuclear area (Fig. 1f).

Evaluation of ELISA system

To assess the clinical potential of our ELISA system, we compared our ELISA system with an existing commercial ELISA kit (Fujirebio Diagnostics, Malvern, PA). We set the cutoff point of the existing ELISA kit as 150 pM based on the manufacturer's instructions (94.4 percentile of healthy individuals). In accordance with the existing ELISA kit, we set the cutoff point of our ELISA system as 5.5 ng/ml based on 94.4 percentile of 37 healthy individuals. We measured concentrations of HE4 of ovarian cancer patients by using two ELISA and found that our ELISA system shows better sensitivity for diagnosis of ovarian cancer than the existing ELISA kit by Fisher's exact probability test ($p<0.05$) (Fig. 2).

Diagnostic value of HE4

We measured serum HE4 levels in cancer patients and healthy controls by using our ELISA system. Mean serum HE4 levels in patients with non-small cell lung cancer, small cell lung cancer, ovarian cancer, gastric cancer, colorectal cancer and healthy adults were 13.3 ng/ml, 17.3 ng/ml, 10.9 ng/ml, 7.2 ng/ml, 7.7 ng/ml and 2.7 ng/ml (Table 1). Serum HE4 levels were significantly higher for non-small, small cell lung cancer and ovarian cancer patients than for healthy controls ($p<0.0001$, $p=0.0007$, and $p=0.0386$, respectively) (Fig. 3a).

To assess the clinical potential of HE4, we calculated sensitivities and specificities of HE4. The operating characteristics for HE4 with its cutoff points for achieving the best individual accuracy are shown in Fig. 3b. The AUC for serum HE4 was 0.988 for differentiating lung cancer patients from healthy adults, with a cutoff value of 6.56 ng/ml (sensitivity= 89.8%, specificity=100%) (Fig. 3b). Serum HE4 levels were elevated in 36/40 (90.0%) non-small cell lung cancer patients, 8/9 (88.9%) small cell lung cancer patients, 8/18 (44.4%) ovarian cancer patients, 6/10 (60.0%) gastric cancer patients and 5/8 (62.5%) colorectal cancer patients (Table 1). These results suggest that the sensitivity of HE4 was high in lung cancer patients.

Prognostic value of HE4

Pre- and post-treatment mean HE4 were 23.0 ng/ml (range 8.3–86.5 ng/ml) and 12.6 ng/ml (range 8.2–16.1 ng/ml), respectively, for PR patients, whereas 21.3 ng/ml (range 9.3–28.1 ng/ml) and 23.8 ng/ml (range 14.2–29.1 ng/ml), respectively, for PD patients (Table 3). Post-treatment mean

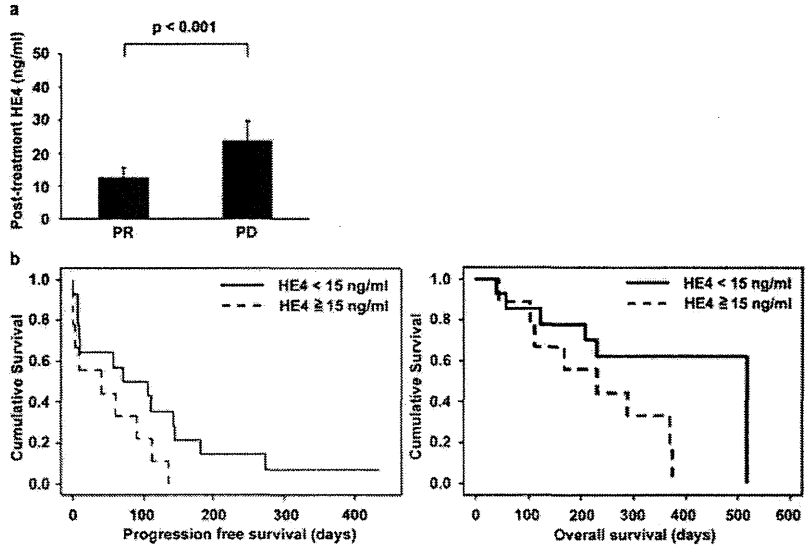

Fig. 4 **a** Post-treatment serum HE4 levels of lung cancer patients receiving chemotherapy. Figures show the average (*columns*) + SD (*bars*). **b** Kaplan–Meier plots of overall survival (*right*) and progression-free survival (*left*) after chemotherapy